

Greenland–Scotland overflow studied by hydro-chemical multivariate analysis

E. Fogelqvist^a, J. Blindheim^b, T. Tanhua^c, S. Østerhus^d, E. Buch^e and F. Rey^b

^a Department of Chemistry, Analytical and Marine Chemistry, Göteborg University, S-412 96, Göteborg, Sweden

^b Institute of Marine Research, P.O. Box 1870, Nordnes, N-5817, Bergen, Norway

^c Institute for Marine Research, Marine Biogeochemistry, Duesternbrooker Weg 20, D-24105, Kiel, Germany

^d Geophysical Institute, University of Bergen, Allégaten 70, N-5007, Bergen, Norway

^e Danish Meteorological Institute, Lyngbyvej 100, Box 1919, DK-2100, Copenhagen K, Denmark

Abstract

Hydrographic, nutrient and halocarbon tracer data collected in July–August 1994 in the Norwegian Sea, the Faroe Bank Channel (FBC), the Iceland and Irminger Basins and the Iceland Sea are presented. Special attention was given to the overflow waters over the Iceland–Scotland Ridge (ISOW). The Iceland–Scotland overflow water (ISOW) was identified along its pathway in the Iceland Basin, and entrainment of overlying water masses was quantified by multivariate analysis (MVA) using principal component analysis (PCA) and Partial Least Square (PLS) calibration. It was concluded that the deeper portion of the ISOW in the FBC was a mixture of about equal parts of Norwegian Sea Deep Water (NSDW) and Norwegian Sea Arctic Intermediate Water (NSAIW). The mixing development of ISOW during its descent in the Iceland Basin was analysed in three sections across the plume. In the southern section at 61° N, where the ISOW core was observed at 2300 m depth, the fraction of waters originating north of the ridge was assessed to be 54%. MVA assessed the fractional composition of the ISOW to be 21% NSDW, 22% NSAIW, 18% Northeast Atlantic Water (NEAW), 11% Modified East Icelandic Water, 25% Labrador Sea Water (LSW) and 3% North East Atlantic Deep Water. It may be noted that the fraction of NEAW is of the same volume as the NSDW. On its further path around the Reykjanes Ridge, the ISOW mixed mainly with LSW, and at 63°N in the Irminger Basin, it was warmer and fresher ($\theta=2.8^{\circ}\text{C}$ and $S=34.92$) than at 61°N east of the ridge ($\theta=2.37^{\circ}\text{C}$, $S=34.97$).

The most intensive mixing occurred immediately west of the FBC, probably due to high velocity of the overflow plume through the channel, where annual velocity means exceeded 1.1 ms^{-1} . This resulted in shear instabilities towards the overlying Atlantic waters and cross-stream velocities exceeding 0.3 ms^{-1} in the bottom boundary layer.

The role of NSAIW as a component of ISOW is increasing. Being largely a product of winter convection in the Greenland Sea when no Greenland Sea Deep Water (GSDW) is formed, it spreads above the older and denser deep water in the Nordic Seas. Little or no GSDW, which earlier was considered to be the principal overflow water, has been formed since 1970. This shows that the Iceland–Scotland overflow may also be maintained with intermediate waters as the principal overflowing component.

Decadal variability in ISOW properties has not been insignificant, as since the early 1960s there has been a decrease in salinity and temperature, by 0.06 and up to 0.5°C , respectively. Such a trend applies also to the LSW, particularly in the Irminger Basin, where it was warmer, saltier and less dense in the late 1950s and early 1960s ($\theta\approx 3.5^{\circ}\text{C}$, $S\approx 34.9$, $\sigma_{1.5}\approx 34.64\text{ kgm}^{-3}$) than in 1994 ($\theta\approx 2.9^{\circ}\text{C}$, $S\approx 34.86$, $\sigma_{1.5}\approx 34.69\text{ kgm}^{-3}$).

CFC tracers were used to assign apparent ages of water masses, showing that the NSDW had an apparent age of about 30 years and that the age of Iceland Sea Deep Water exceeded 25 years. NSAIW observed in the southern Norwegian Sea was estimated to be 6–16 years old. An upper age limit of LSW in the Iceland Basin was found to be 18–19 years. It was further concluded that the products of the onset of intense wintertime convection in the Labrador Sea in the late 1980s were not yet observed in the northern central part of the Iceland Basin. The LSW in the Irminger Basin was found to be significantly younger.

Two layers were found there. A shallower layer at a depth of 1000–1500 m depth was older than the layer beneath by about 4 years, while the deeper layer at 1500–1800 m depth was assessed at an apparent age ranging between less than 1 (formed during the previous winter) and 4 years.

Author Keywords: Thermohaline circulation; Overflow; Entrainment; Water masses; CFC tracers; Multivariate analysis; Region: Northern North Atlantic, 60°N–68°N, 0°–35°W

1. Introduction

A driving mechanism for the thermohaline circulation is cooling of surface waters at high latitudes and consequent formation of deep water by sinking of the cooled water masses. In the North Atlantic such deep convection may occur in the Greenland and Labrador Seas as well as in some shelf areas around the Arctic Ocean. It is well known that the overflow originating from the Nordic Seas, which is dealt with here, is split in two. A western component leaves the Iceland Sea through Denmark Strait into the Irminger Basin (see e.g. [Swift et al., 1980](#); [Rudels](#); [Rudels and Rudels](#)), while the other one overflows the ridge between Iceland and Scotland with its main exit through the Faroe Bank Channel (FBC; [Knudsen, 1898](#); [Dooley and Meincke, 1981](#); [Van Aken and Eisma, 1987](#); [Hansen et al., 2001](#)).

A main objective of the present work was to study the mixing of the overflowing waters with water masses south of the Greenland–Scotland Ridge, particularly along the main pathway of Iceland–Scotland overflow water (ISOW) during its descent into the Iceland Basin. This study was based on CTD, nutrient and tracer data from a cruise in July–August 1994. Positions of stations occupied during this cruise, which was a component of the Nordic WOCE project, are presented in [Fig. 1](#).

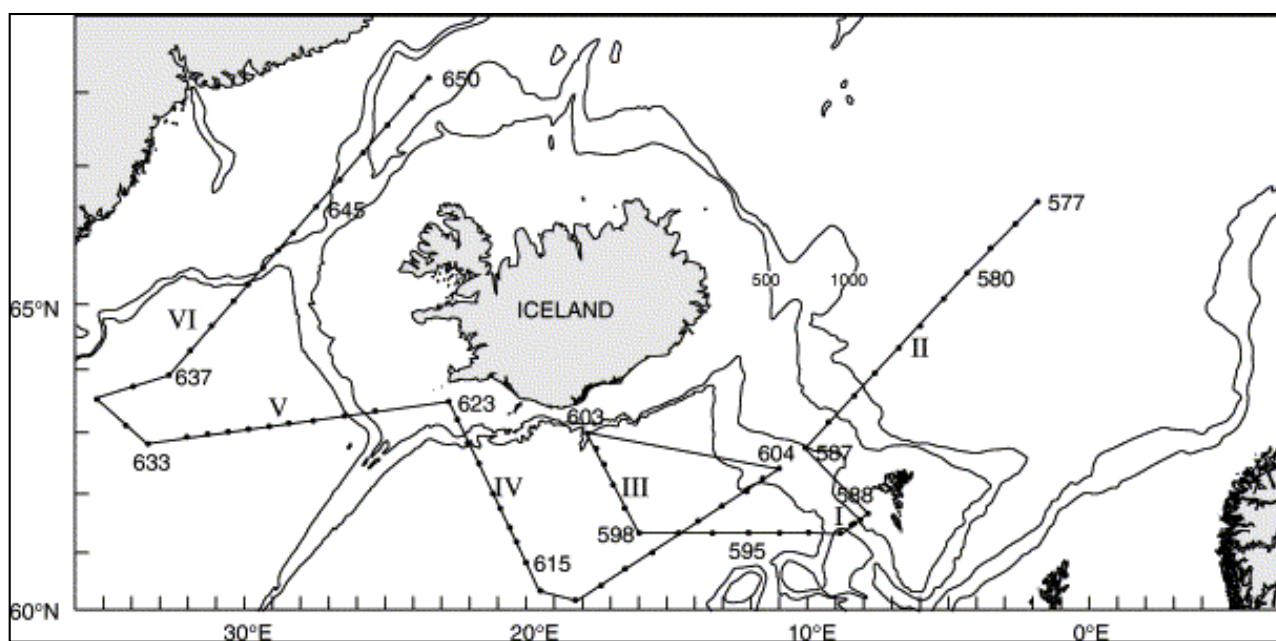


Fig. 1. Cruise track and positions of sections and stations occupied during the Nordic WOCE cruise with R./V. *Johan Hjort*, July 23–August 16, 1994.

A schematic presentation of the circulation and the main features of the bathymetry in the region are shown in [Fig. 2](#). The most important bathymetric feature is the Greenland–Scotland Ridge, which isolates the deeper water masses in the Nordic Seas from the North Atlantic. In contrast to the almost 4000 m deep basins in the Nordic Seas, the deepest passages across the ridge are through the FBC and the Denmark Strait, where the sill depths are about 850 and 620 m, respectively.

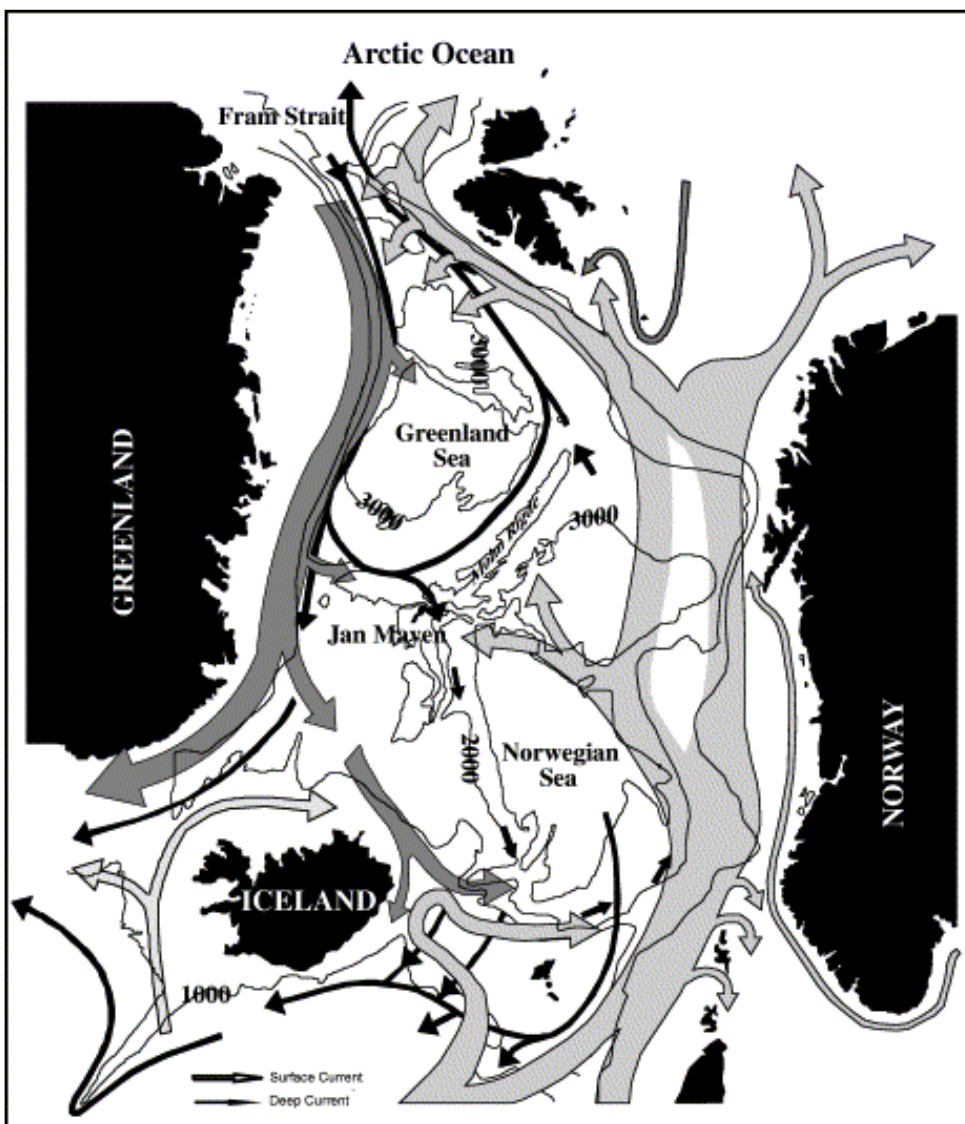


Fig. 2. Major current systems across the Scotland–Greenland ridge and in the Nordic Seas. Dark grey arrows represent cold surface currents, light grey are warm surface currents and black are deep currents.

A major feature south of Iceland is the Reykjanes Ridge. Being a part of the Mid-Atlantic Ridge, it forms the bordering structure between Irminger Basin on its western side and the Iceland Basin to the east, and it is decisive for the circulation in both these basins. South of the Reykjanes Ridge, at about 52°N, the Charlie–Gibbs Fracture Zone cuts through the mid-ocean ridge, and forms a more than 3000 m deep connection between the eastern and western basins in the North Atlantic.

The Nordic Seas, north of the ridge, are characterised by a large-scale cyclonic circulation. To the east, the Atlantic waters of the Norwegian Atlantic Current and the West Spitsbergen Current flow northward, while the East Greenland Current (EGC) characterises the western side, carrying cold waters southward. Basin-scale cyclonic circulation brings both Atlantic and Arctic waters into the interior of the basins.

The strong winter cooling in the area produces very cold and dense deep waters of relatively constant properties, although small decadal variations occur (compare e.g. [Aagaard, 1968](#); [Clarke et al., 1990](#)) and the depth of the winter convection may vary considerably between years. A further feature observed since about 1980 is the occurrence of Arctic intermediate waters spreading eastward from the Greenland and Iceland Seas, intruding under the Atlantic water in the eastern part of the area.

In the upper layers of the Iceland Basin the predominant flow of relatively salty and warm water from the North Atlantic Current is towards the north, but along the eastern side of the Reykjanes Ridge there are, at least periodically, indications of a southward flow ([Otto and van Aken, 1996](#); see also [Hansen and Østerhus, 2000](#)). In the Irminger Basin there is a northward current of Atlantic water along the western side of the Reykjanes Ridge. This is the Irminger Current, which bifurcates in the Denmark Strait with one branch going into North Icelandic shelf waters while the other turns southwest to continue along the East Greenland slope. There it flows parallel with, and intrudes underneath, the cold waters of the EGC, which are carried southward from their main source in the Arctic Ocean. Below the Atlantic waters, Labrador Sea Water (LSW) is the dominating intermediate water mass in both basins, where it is characterised by a salinity minimum. The bottom water in the

Iceland Basin has mostly the characteristics of Northeast Atlantic Deep Water (NEADW; Lee and Ellett, 1967) while the bottom layers of the northern Irminger Basin are dominated by the overflowing water masses. Here we adopt the nomenclature used by Lee and Ellett (1967). McCartney (1992) applied the term "Lower Deep Water" (LDW) for deep waters south of the Iceland Basin, but further north in the southern Iceland Basin he called it LDW influenced bottom water.

Water masses are further described below in separate sections on the area north of the Greenland–Scotland Ridge, the Iceland Basin and the Irminger Basin. Properties of the various water masses as applied in this work are also presented in Table 1.

Table 1. Physical and chemical properties of some water masses in the studied area, appearing in alphabetic order

<i>Denmark Strait Overflow Water (DSOW)</i>			
Water flowing through the Denmark Strait, and sinking to the bottom of the Irminger Basin. It originates mainly from intermediate waters in the Iceland Sea and the East Greenland Current. Short-term variability is considerable over the sill. The data entered here are based on observations close to the lower Greenland slope in Sections V and VI.	<i>S</i>	34,84–34,87	
	θ	0,7–1,9	°C
	O ₂	296–311	μmol kg ⁻¹
	Si	8–10	
	NO ₃	13,2–14,4	
	PO ₄	1,0–1,1	
	CFC-11	4,0–4,5	pmol kg ⁻¹
	CFC-12	1,2–1,7	
	CFC-113	0,2–0,4	
	CCl ₄	4,8–5,5	
<i>Iceland Sea Arctic Intermediate Water (ISAIW)</i>			
This water mass is mainly formed by winter convection in the northern/central Iceland Sea, although mixed with similar intermediate water derived from the Greenland Sea. It is also known as upper Arctic Intermediate Water (Swift and Aagaard, 1981; chemical and tracer data from the present data set)	<i>S</i>	34,7–34,9	
	θ	< 2	°C
	O ₂	310–330	μmol kg ⁻¹
	Si	6–8	
	NO ₃	12,5–13,2	
	PO ₄	0,8–1,0	
	CFC-11	4–5,5	pmol kg ⁻¹
	CFC-12	1,7–2,2	
	CFC-113	0,3–0,5	
	CCl ₄	5,5–8	

	CFC-12	1.7–2.2	
	CFC-113	0.3–0.5	
	CCl ₄	5.5–8	
<i>Iceland Sea Deep Water (ISDW)</i>			
This water mass is very similar to NSDW, but has a slightly higher salinity due to larger admixture of deep water from the Arctic Ocean. (Buch et al., 1992)	S	34.910–34.912	
	θ	~ -1	°C
	O ₂	290–300	$\mu\text{mol kg}^{-1}$
	Si	10–12	
	NO ₃	~ 14.3	
	PO ₄	0.9–1.1	
	CFC-11	1.1–1.4	pmol kg^{-1}
	CFC-12	0.4–0.6	
	CFC-113	Not detectable	
	CCl ₄	1.9–2.5	
<i>Iceland–Scotland Overflow Water (ISOW) in the Irminger Basin</i>			
Water that overflows the Iceland–Scotland Ridge, mainly through the Farøe Bank Channel. The water mass is transported into the Irminger Basin around the Reykjanes Ridge, mainly through the Charlie–Gibbs Fracture Zone.	S	~ 34.92	
	θ	2.7–2.9	°C
	O ₂	275–280	$\mu\text{mol kg}^{-1}$
	Si	12–13	
	NO ₃	15.9–16.0	
	PO ₄	~ 1.2	
	CFC-11	1.9–2.2	pmol kg^{-1}
	CFC-12	0.7–0.9	
	CFC-113	Not detectable	
	CCl ₄	3.0–3.3	
<i>Irminger Sea Water (ISW)</i>			
Upper water in the northern Irminger Basin. It is an Atlantic water mass that is mainly supplied by the Irminger Current.	S	35.05–35.10	
	θ	5–7	°C
	O ₂	275–280	$\mu\text{mol kg}^{-1}$
	Si	7–8	
	NO ₃	14.6–15.0	
	PO ₄	1.0–1.1	
	CFC-11	4.4–4.6	pmol kg^{-1}
	CFC-12	1.6–1.9	
	CFC-113	~ 0.3	
	CCl ₄	4–5	

Labrador Sea Water in the

	CFC-113	~ 0.3	
	CCl ₄	4-5	
<i>Labrador Sea Water in the Iceland Basin (LSW_E)</i>			
This water originates from deep convection in the Labrador Sea. It advects into the Iceland Basin below the Atlantic water. Due to greater distance from its origin, its properties are somewhat different from LSW advecting into the Irminger Basin.	S	34.8-34.9	
	θ	3.0-3.5	°C
	O ₂	270-280	$\mu\text{mol kg}^{-1}$
	Si	11-12	
	NO ₃	16.1-17.0	
	PO ₄	~ 1.2	
	CFC-11	2.2-2.4	pmol kg^{-1}
	CFC-12	1.0-1.5	
	CFC-113	~ 0.1	
	CCl ₄	3.0-3.5	
<i>Labrador Sea Water in the Irminger Basin (LSW_W)</i>			
This water has the same source in the Labrador Sea as the LSW _E . The transport time is shorter and the water has higher CFC contents.	S	< 34.9	
	θ	2-3	°C
	O ₂	290-300	$\mu\text{mol kg}^{-1}$
	Si	10-11	
	NO ₃	16.1-16.3	
	PO ₄	1.1-1.2	
	CFC-11	3.8-4.8	pmol kg^{-1}
	CFC-12	1.3-2.3	
	CFC-113	0.20-0.35	
	CCl ₄	5-6	
<i>Modified East Icelandic Water (MEIW)</i>			
This is a mixture of water mass modifications in the area of the East Icelandic Current. (Read and Pollard, 1992; chemical and tracer data from present data set)	S	34.6-34.9	
	θ	1-3	°C
	O ₂	~ 300	$\mu\text{mol kg}^{-1}$
	Si	6-7	
	NO ₃	13.1-13.6	
	PO ₄	~ 1	
	CFC-11	5.5-6.7	pmol kg^{-1}
	CFC-12	~ 2.8	
	CFC-113	0.3-0.4	
	CCl ₄	7-9	

	CFC-12	~ 2.8	
	CFC-113	0.3–0.4	
	CCl ₄	7–9	
<i>Northeast Atlantic Deep Water (NEADW)</i>			
The bottom water of the Iceland Basin (Lee and Ellett, 1967). McCartney (1992) mentioned it as Lower Deep Water influenced bottom water. Lower Deep Water occurs south of the Iceland Basin.	S	34.95–35.0	
	θ	2–3	°C
	O ₂	270–280	$\mu\text{mol kg}^{-1}$
	Si	13–17	
	NO ₃	15.0–16.0	
	PO ₄	1.1–1.2	
	CFC-11	1.7–2.1	pmol kg^{-1}
	CFC-12	0.8–1.1	
	CFC-113	< 0.1	
	CCl ₄	2.5–3.0	
<i>Northeast Atlantic Water (NEAW)</i>			
Lee and Ellett (1965) defined T/S properties of North Atlantic Water in the vicinity of the Farøe Islands to be 9°C/35.33, which in the present data set are associated with 8–10°C/35.20–35.34.	S	~ 35.3	
	θ	8–10	°C
	O ₂	265–270	$\mu\text{mol kg}^{-1}$
	Si	3–6	
	NO ₃	12.5–13.5	
	PO ₄	0.9–1.0	
	CFC-11	3.8–4.2	pmol kg^{-1}
	CFC-12	1.2–2.5	
	CFC-113	0.2–0.4	
	CCl ₄	3.0–4.5	
<i>Norwegian Sea Arctic Intermediate Water (NSAIW)</i>			
NSAIW advects from the Greenland and Iceland seas into the Norwegian Sea where it occurs in a layer identified by a salinity minimum between the upper layers, mainly of Atlantic water, and the deep water.	S	34.87–34.90	
	θ	$-0.5 < \theta < 0.5$	°C
	O ₂	294–302	$\mu\text{mol kg}^{-1}$
	Si	7.0–8.4	
	NO ₃	14.1–14.5	
	PO ₄	1.0–1.1	

	Si	7.0–8.4	
	NO ₃	14.1–14.5	
	PO ₄	1.0–1.1	
	CFC-11	3.5–4.0	pmol kg ⁻¹
	CFC-12	1.6–2.0	
	CFC-113	0.1–0.2	
	CCl ₄	4.0–5.5	
<i>Norwegian Sea Deep Water (NSDW)</i>			
True NSDW is found at depths greater than approximately 2500 m in the Norwegian Sea. At these depths it is close to homogeneous in salinity and adiabatically isothermal.	S	~ 34.91	
	θ	~ -1.03	°C
	O ₂	297–299	μmol kg ⁻¹
	Si	~ 13	
	NO ₃	15.0–15.6	
	PO ₄	1.1–1.2	
	CFC-11	0.2–0.5	pmol kg ⁻¹
	CFC-12	No data	
	CFC-113	Not detectable	
	CCl ₄	1.3–1.6	
<i>Polar Intermediate Water (PIW)</i>			
PIW is represented by a temperature minimum underneath the upper waters of the East Greenland Current. Distinguished from ISAIW mainly by geographic distribution (e.g. Malmberg, 1972 and Fogelqvist, unpublished data). Nutrient and tracer data are based on observations north of the sill in Section VI.	S	34.4–34.7	
	θ	< 0	°C
	O ₂	327–329	μmol kg ⁻¹
	Si	~ 7	
	NO ₃	11.9–12.3	
	PO ₄	0.9–1.0	
	CFC-11	5.7–6.0	pmol kg ⁻¹
	CFC-12	2.1–2.6	
	CFC-113	0.3–0.5	
	CCl ₄	8.0–9.0	
<i>Polar Water (PW)</i>			
This water mass is carried into the area by the East Greenland Current. The salinity is low and variable due to melting of Ice and a contribution of Arctic Ocean surface water (e.g. Malmberg 1972). Nutrient and tracer data are based on observations north of the	S	< 34.4	

Ocean surface water (e.g. Malmberg 1972). Nutrient and tracer data are based on observations north of the sill in Section VI.

θ	0°C	
O ₂	330–370	$\mu\text{mol kg}^{-1}$
Si	< 7	
NO ₃	< 11	
PO ₄	< 0.9	
CFC-11	6.0–6.9	pmol kg^{-1}
CFC-12	2.1–2.6	
CFC-113	0.4–0.6	
CCl ₄	7.3–8.6	

Return Atlantic Water (RAW)

This water of Atlantic origin has circulated into the EGC from the Spitsbergen Current and the Atlantic layer in the Arctic Ocean (Rudels et al., 1999c; and Tanhua, unpublished data). This water mass is not covered by the present data. Data from 1997 R./V. *Aranda* cruise to Denmark Strait.

S	34.9–35.0	
θ	0–2	°C
O ₂	300–310	$\mu\text{mol kg}^{-1}$
Si	5.5–6.0	
NO ₃	~ 12	
PO ₄	~ 0.8	
CFC-11	4.9–5.2	pmol kg^{-1}
CFC-12	2.2–2.7	
CFC-113	0.30–0.35	
CCl ₄	5.4–5.7	

Properties are from the present data set when no reference is entered.

Along the topographically controlled pathway through the Iceland Basin, the properties of the overflowing water are gradually changed by mixing with the basin water masses. This results in a relatively homogeneous water type called ISOW (e.g. Ellett and Martin, 1973; Schmitz and McCartney, 1993). During the descent of the Denmark Strait Overflow Water (DSOW) there is less entrainment of the water masses in the Irminger Basin. Therefore, relatively undiluted DSOW may reach the basin floor. The reason for this seems to be that some DSOW reaches the basin floor after being mixed only with less dense, low salinity water within the plume (Rudels et al., 1999b).

The intensity of the entrainment of ambient waters into the overflow water is illustrated by the volume transport estimates given by Dickson et al. (1990). Based on current measurements between 62°N and 64°N off East Greenland, they found a deep water volume transport along the continental slope amounting to 10.7 Sv. This means that the volumes of Iceland–Scotland Overflow of 2.5–3.0 Sv (Saunders, 1990; Borenäs and Lundberg, 1988; Hansen and Østerhus, 2000) together with the Denmark Strait Overflow of about 3 Sv (Ross, 1984; Hansen and Østerhus, 2000) have approximately doubled by entrainment of ambient waters.

Water mass classification has traditionally been based upon temperature and salinity characteristics, in some cases together with oxygen and nutrients. In recent years chemical tracers have also contributed to water mass classification. An objective of the present work was to identify the source waters of the overflow and to assess the fractional composition of the overflow water masses near the sills across the ridge as well as further downstream. To obtain this we applied multivariate analysis

(MVA) to the data, using all the observed variables in the analyses: temperature, salinity, oxygen, nutrients and chlorofluorocarbons (CFCs).

MVA was applied to describe the evolution of the ISOW during its descent into the Iceland Basin, where it is modified by mixing with the water masses in the basin: Northeast Atlantic Water (NEAW), LSW, NEADW and, possibly, to a small extent, Mediterranean Water (Harvey and Theodorou, 1986).

The CFC data are also applied for estimates of apparent ages, that is, the time since they were at the surface and equilibrated with the atmosphere, and transport times of some water masses. The atmospheric concentrations of these tracers have increased since they were introduced until around 1990. Thus any relatively recently ventilated water mass carries a time specific signature of CFC tracers, which facilitates the age determination of that water parcel. The atmospheric history of the CFC tracers is given by Walker et al. (2000), the solubilities of CFC-11 and CFC-12 by Warner and Weiss (1985), and the solubility of CFC-113 by Bu and Warner (1995). The ages reported from the data set collected in July–August 1994 are based on the CFC tracer measurements. Temporal variations in the properties of some of these water masses are assessed by comparison with earlier studies.

2. Data collection and analysis

A total of 74 stations were occupied along the cruise track shown in Fig. 1. A SeaBird 911 CTD system with dual temperature and conductivity sensors, equipped with a 12-position SeaBird Carousel Sampler with 10 l Niskin bottles, was used for the observational work. Double casts were applied at most stations where samples for transient tracers were drawn. Information from the previous stations as well as knowledge of the hydrographic structure was applied when sampling depths were decided on stations with only one cast. Pre- and post-cruise calibrations of the thermometers at the SeaBird calibration facility indicated insignificant drift during the cruise and an accuracy of both thermometers within 0.001°C. Parallel calibrations of the conductivity sensors for salinity measurements also showed insignificant drift during the cruise. Based on these calibrations supported by corrections obtained from salinity samples analysed onboard with an 8400 Autosol salinometer, CTD salinities were also accurate within 0.001 units.

In addition to CTD profiles and salinity samples, water was sampled for measurements of halocarbons, dissolved oxygen, nitrate, nitrite, phosphate, silicate, partial pressure of carbon dioxide, total dissolved inorganic carbon, and, at a few stations, tritium, helium, ¹³C and ¹⁴C.

Sub-samples for halocarbon determinations were drawn into 100 ml ground glass syringes and stored under seawater prior to analysis, which was performed within 5 h of sampling. The halocarbons were measured with purge and trap sample work-up followed by gas chromatographic separation and electron capture detection. The method of halocarbon analysis is described in more detail elsewhere (Fogelqvist, 1999). The halocarbons were standardised against a gas standard supplied by the Plymouth Marine Laboratory, England, and the calibration curves were fitted to a polynomial function of the third order. The CFC data were calibrated against the SIO-93 calibration scale. Sample to sample precision and limits of detection are reported in Table 2.

Table 2. Precision and limits of detection for the two parallel channels of the analytical system for halocarbon measurements

Tracer	Precision Channel A (%)	Precision Channel B (%)	Limit of detection (pmol kg ⁻¹)
CFC-11	0.8	1.0	0.02
CFC-12	1.0	1.5	0.04
CFC-113	6.0	2.4	0.06
CCl ₄	1.1	1.1	0.02

2.1. Multivariate analysis of oceanographic data

Water mass classification has traditionally been based upon temperature and salinity characteristics, in some cases together with oxygen and nutrients. In recent years measurements of chemical tracers, such as the CFCs, isotopes of carbon (¹⁴C), krypton (⁸⁵Kr), tritium (³H), caesium (¹³⁷Cs) and strontium (⁹⁰Sr), have contributed to water mass classification. By using multivariate analyses, which are statistical methods for simultaneous treatment of several parameters, an improved water mass identification can be obtained, which also leads to better estimates of the mixing between the various water masses.

Tomczak (1981a) used multiparameter analysis as an extension of TS analysis, and this method is applied to mixing calculations in various parts of the ocean (Tomczak, 1981b; Tomczak and Large, 1989; Hinrichsen and Tomczak, 1993). In a further extension of this method, optimum multiparameter analysis is combined with CFC and oxygen mixing analysis to determine the ages of water masses (Karstensen and Tomczak, 1998). Mackas et al. (1987) used a method based on least squares regression analysis applied to oceanographic data. In a recent work (Min, 1999), a multiparameter analysis method is used to calculate the composition of the "Middle Irminger Water".

The method of principle component analysis (PCA) in oceanographic and meteorological applications is described in Preisendorfer (1988). For this work we used the software "Unscrambler" Version 5.5, CAMO AS, Trondheim, Norway, to perform the MVA. We give only a rather brief review of the theory behind MVA here, as it is quite extensive and not within the scope of the current paper. For principles of and for practical instructions on MVA, see Esbensen et al. (1994) and Martens and Naes (1989).

MVA is a method for handling large numbers of variables and compilation of all varying data into a few trends and a noise residual, making further mathematical treatment simple and numerically stable. We treated data in a two-step procedure, in which PCA is the first step. PCA can be used to identify the most influential variables, to find patterns within the data set and to classify objects into groups. (In the context of statistical treatment of the data in this work, a variable is equivalent to a measured parameter, whereas the objects are the individual water samples.) This arrangement of data constitutes the base for a partial least square (PLS) calibration, which makes predictions and interpretations from the data set.

PCA mathematically transforms the data set into orthogonal base vectors (principal components, PCs) plus a residual part, which can be regarded as noise. The first PC is the vector that minimises the squared projection distances from the data points to the line. The first PC then contains most of the information of the PCs of a data set, or rather, the most variance within the data set. The PCs are calculated one at a time, recursively, until all of the variance is explained. In this study PCA was used to identify specific samples representative of typical water masses, to detect outliers and to find which variables optimally describes the variance of the data set. The outcome of PCA is the same number of PCs as there originally were variables. However, the first few PCs contain most of the information; the remaining ones represent mainly the noise. Consequently, PCA makes the data set more manageable by decomposing it to fewer dimensions, with little loss of information. In the case of this specific data set, 10 variables were used for the PCA, and typically around 95% of the variance of the data could be explained by the first three PCs. By plotting the most influential PCs versus each other, often in a 3D plot, it is not difficult to identify end members, i.e. samples at the ends of mixing lines. The characteristics of the end members are then signatures of the water masses present in that particular data set; we can call them "source waters" for this discussion. This process is similar to identification of water masses on a TS plot. By using a few water samples, typically 3–5, rather than a single value to represent a particular water mass, the variability within that water mass is accounted for in the analysis. This is an important feature of the MVA as compared to classical TS analysis. All the water samples in that area are then considered as mixtures of the source waters. Properties of all water masses relevant for the MVA or age assessments in the Nordic Seas, the Iceland Basin and the Irminger Basin are entered in Table 1, but in the MVA on a particular section, only water masses influencing that section were applied.

After the source waters have been defined, a calibration model is made in a second operation by a PLS technique, whereby the fractions of the source waters can be estimated by a process called prediction for each water sample. PLS involves two sets of data, one *X* matrix containing independent variables (the measurements) and one *Y* matrix with the dependent data (e.g. the water mass composition). PLS performs a simultaneous and interdependent decomposition of both *X* and *Y* matrices in order to obtain this calibration. This is done in such a way that the information in the *Y* matrix is used directly as a guide for optimal decomposition of the *X* matrix. PLS can be regarded as an extension of PCA, with the difference that in PLS the criterion for significance is the ability of the calibration to predict the *Y* matrix. As an example, the *X* matrix can consist of salinity, temperature and CFC-11, while the *Y* matrix defines the chosen source waters from the same variables. Once a calibration is done, it is applied to the data set, and the fractions of the different source waters in each individual water sample are determined. Multivariate analysis is insensitive to what process leads to mixing of the water masses. On the contrary, it proved to be a useful method for estimating flow patterns and mixing independent of the mixing process.

The general procedure was the following. The parameters available to characterise a water sample were in almost all cases 10: salinity, temperature, oxygen, silicate, nitrate, phosphate and four halocarbons (CFC-11, CFC-12, CFC-13 and CCL₄).

Fewer variables were applied only exceptionally. For example, there were not values of CFC-12 available in NSDW because the analysis of these samples did not meet the quality requirements. All the 10 parameters did provide information to the water mass definitions, even though many of these parameters provide information that is similar. The halocarbon tracers and the three measured nutrients, for example, provide similar information, but not identical, and it is justified to include all of them as long as the precisions of the measurements are similar. After PCA modelling, a number of characteristic water

samples were identified (at the ends of mixing lines) representing the source waters, from which a calibration model was created by setting each source water to be 100% pure. It is important to note that more than one data point is used to characterise a water mass. The method of PLS thereby accounts for the natural variability of the water mass. It is also worth noting that we use only water samples from the present survey to define water masses; we do not use the concept of water types that represent a point in parameter space. The water mass analysis we perform is independent of the formation process for the water masses. The purpose of this analysis is mainly to study the mixing in water masses within a limited region, and it is therefore justified to use the water masses as they appear on the edges of our study area as typical source waters for our water mass analysis. It is also worth noting that not all water masses indicated in [Table 1](#) are used in each analysis; instead only the water masses that are expected to contribute to the mixing in each area are included in the analysis. As a matter of fact, the MVA seems to have difficulties in handling areas where more than five water masses mix with each other, and each area needs to be treated with its own MVA. The PLS prediction gives as a result the percentages of all source waters in each sample.

The uncertainty in the prediction of water mass composition by PLS is a combination of two sources of errors: the model itself and the errors of the parameters used for the calibration. The first estimate of uncertainty is the prediction error of the model, the root mean square error of prediction (RMSEP). It is based on a cross validation of the model with a random selection of calibration samples. The squared difference between measured and modelled results is used for the calculation of the RMSEP. After the PLS calibration, the program reports on each individual result's deviation from the model, which is a measure of the uncertainty reflecting partly the construction of the calibration model and the variation in calibration samples, and partly the uncertainty of the data that are calibrated. RMSEP values as well as mean deviations of prediction results are presented in [Table 3](#).

Table 3. Estimates of uncertainties of the PCA/PLS calibrations of fractional percentages

Iceland Sea			Norwegian Sea			Farøe Bank Channel		
Water mass	RMSEP (%)	Mean dev. (%)	Water mass	RMSEP (%)	Mean dev. (%)	Water mass	RMSEP (%)	Mean dev. (%)
ISW	4.15	5.29	MEIW	8.70	6.99	MEIW	8.70	4.17
ISAIW	7.38	9.71	NEAW	4.58	3.29	NEAW	4.58	4.68
ISDW	6.53	9.96	NSAIW	11.3	8.31	NSAIW	11.3	9.62
			NSDW	5.53	3.99	NSDW	5.53	6.47

MVA was especially useful for the study of the water mass composition in the overflow from the Nordic Seas across the Iceland–Scotland Ridge. The multivariate method, however, has its limitations when used for systems as complex as the mixing pattern of several water masses, especially if the source waters have similar properties. This is illustrated in [Table 3](#), where the uncertainties, the RMSEP values, are higher for NSAIW and Modified East Iceland Water (MEIW) than for the other water masses. Any attempt to simultaneously resolve all the water masses in any of the basins south of the ridge caused uncertainties in the predictions that are too large to justify any firm conclusions. The main reason for this uncertainty is the large number of water masses in the basins, some of them with properties that are quite similar. An exception is the plume of overflow water in the Iceland Basin emanating from the FBC, which has characteristics sufficiently different from the other water masses in the basin (see discussion below).

3. Results and discussion

The water masses that are of importance in the overflow process are those that form the sources of the overflow and those modifying the overflow along its pathway. The source water masses are formed north of the Greenland–Scotland Ridge; the modifying waters consist of intermediate, deep and bottom water masses south of the ridge. These are somewhat different in the Iceland–Scotland overflow in comparison with the Denmark Strait overflow. Therefore, the different basins are discussed separately, starting from the Nordic Seas ([Fig. 4](#) and [Fig. 8](#)), through the FBC ([Fig. 3](#)) into the Iceland Basin ([Fig. 4](#), [Fig. 5](#) and [Fig. 6](#)), and further to the Irminger Basin ([Fig. 7](#) and [Fig. 8](#)). The discussion is focused on the results from the CTD and halocarbon measurements, even if nutrient and oxygen data have been used for classification of water masses and for the MVA of the results.

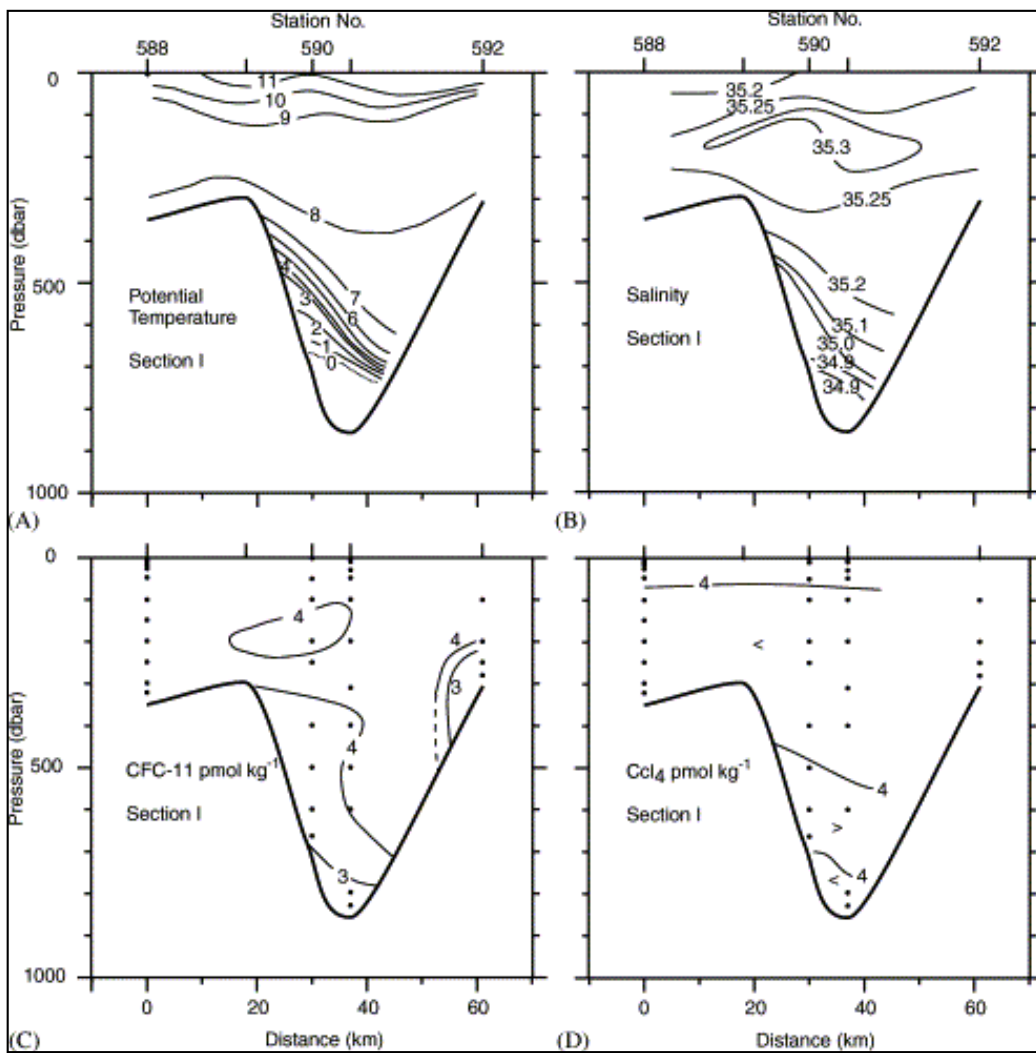


Fig. 3. Section I across the Faroe Bank Channel, Stations 588–592. Distribution of (A) potential temperature, (B) salinity, (C) CFC-11, and (D) CCl_4 .

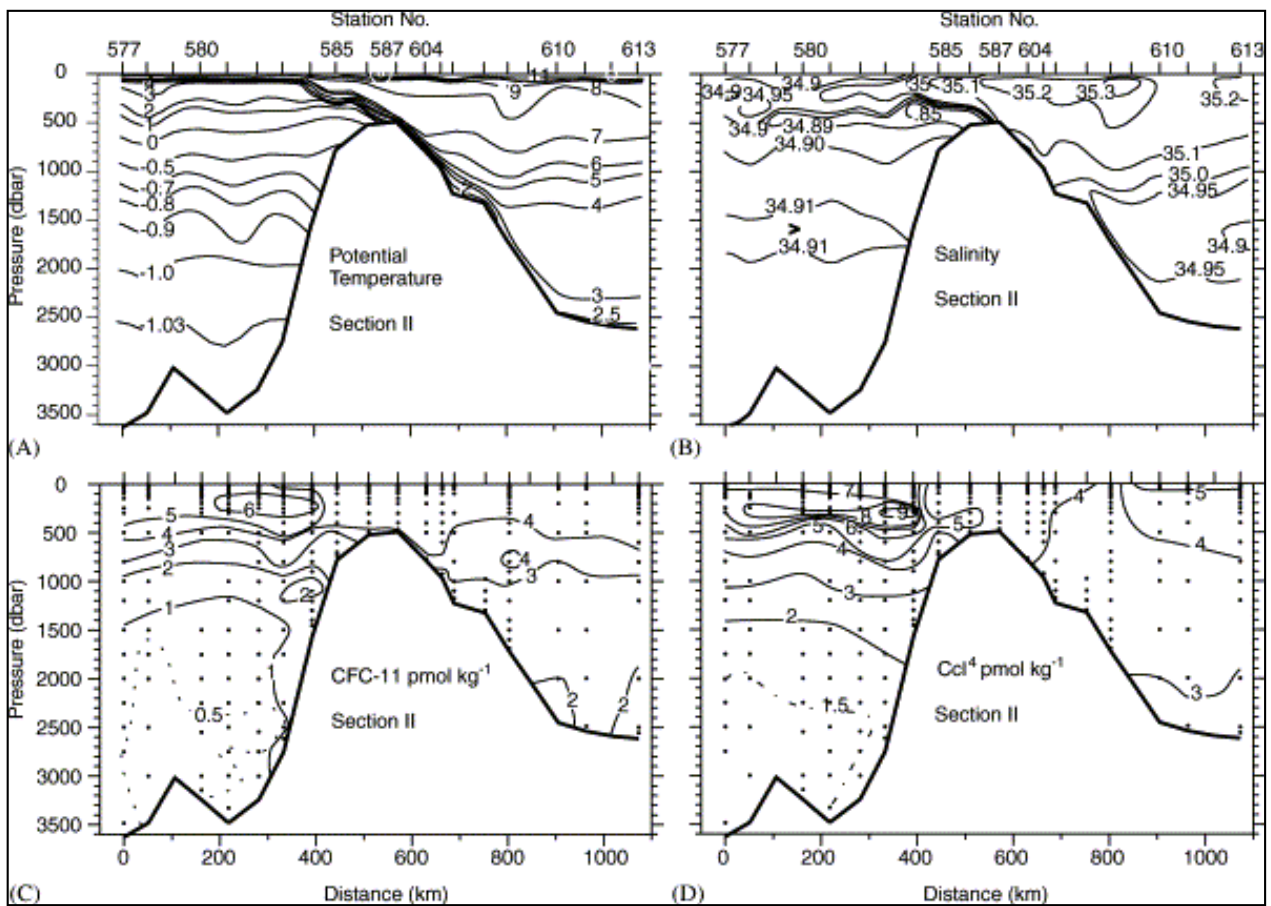


Fig. 4. Section II from the Norwegian Sea (Station 577) over the Iceland–Faroe Ridge to the Iceland Basin (Station 613). Distribution of (A) potential temperature, (B) salinity, (C) CFC-11, and (D) CCl_4 .

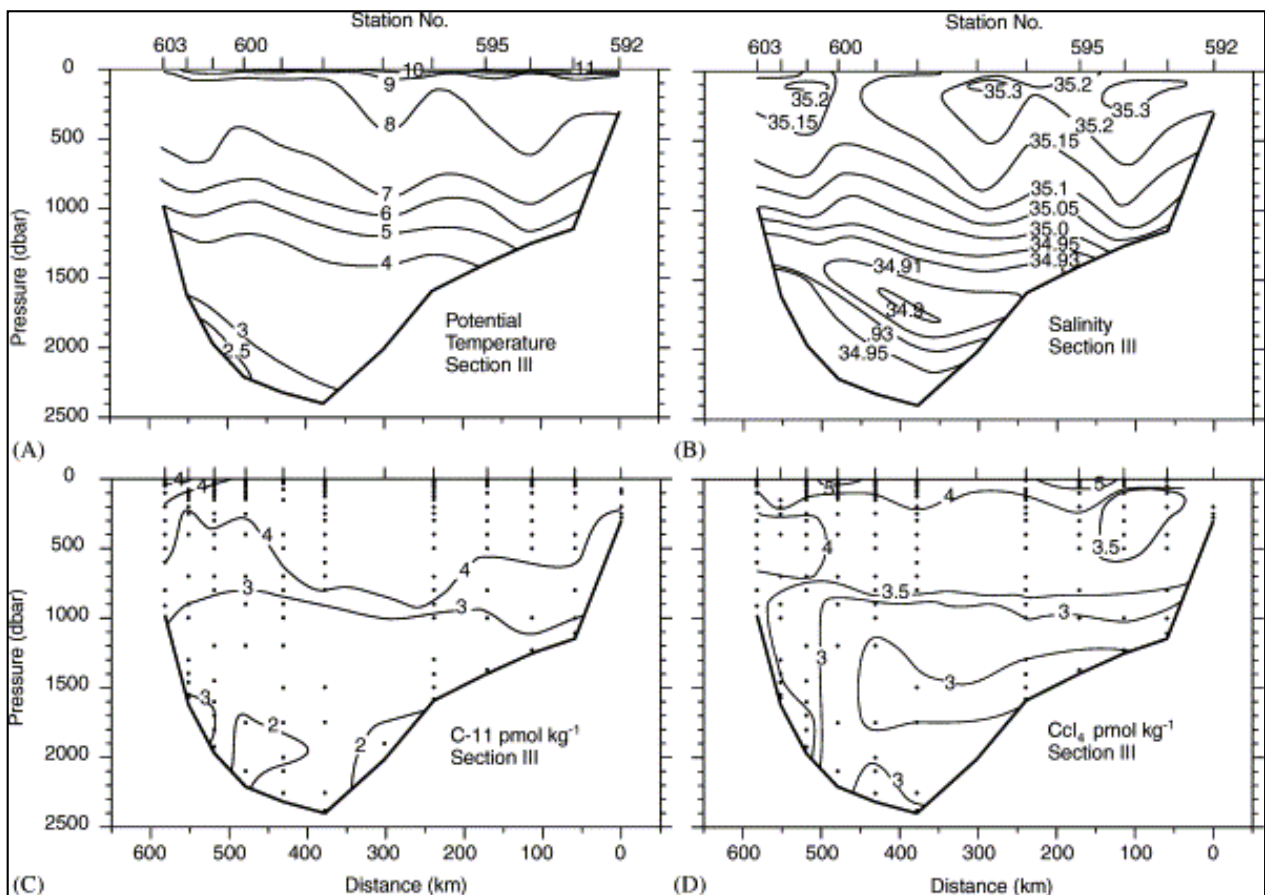


Fig. 5. Section III through the Iceland Basin from the Faroe Bank Channel (Station 592) to the Icelandic coast (Station 603). Distribution of (A) potential temperature, (B) salinity, (C) CFC-11, and (D) CCl_4 .

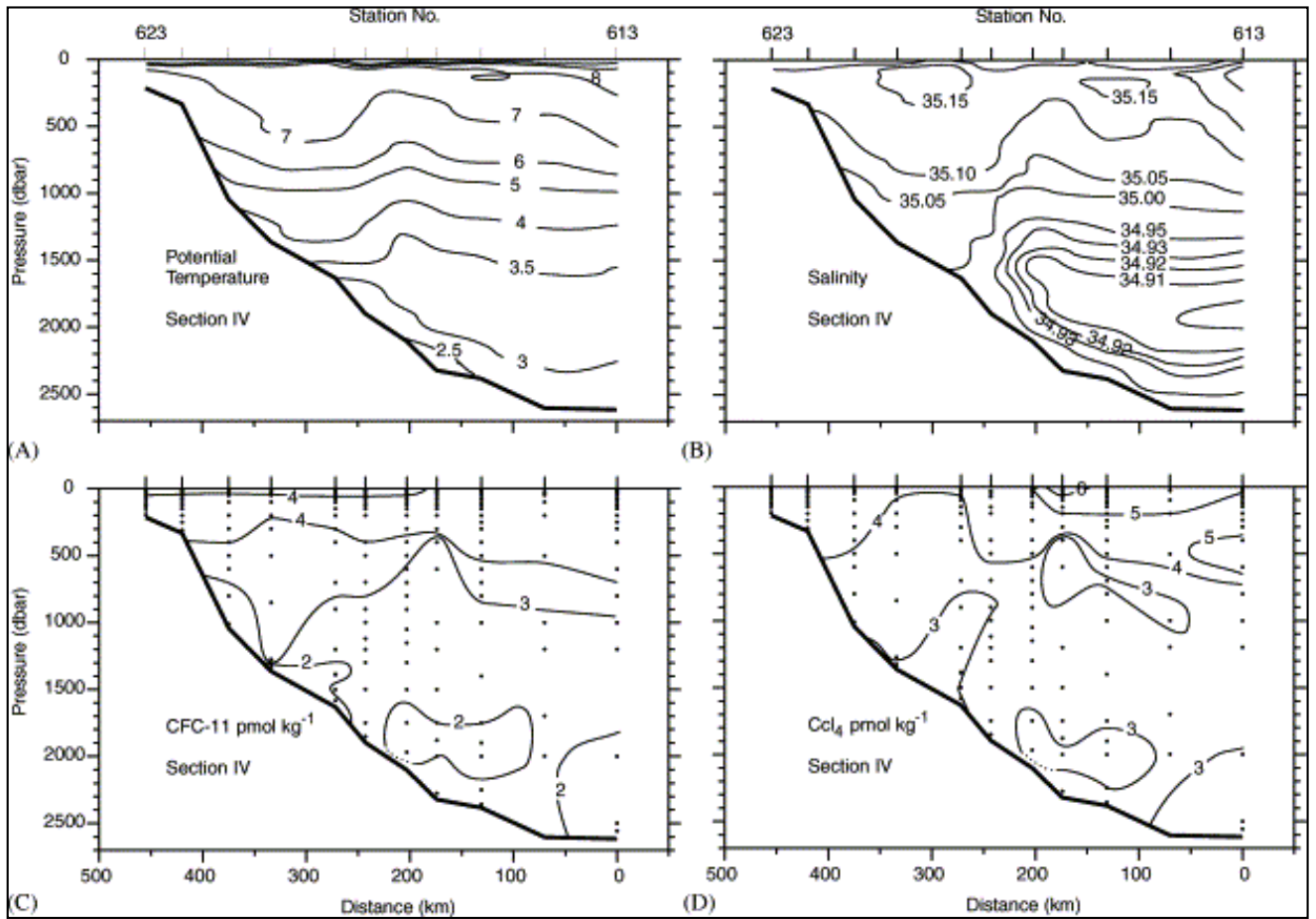


Fig. 6. Section IV across the slope south of Iceland from the Iceland Basin (Station 613) towards Reykjanes (Station 623). Distribution of (A) potential temperature, (B) salinity, (C) CFC-11, and (D) CCl₄.

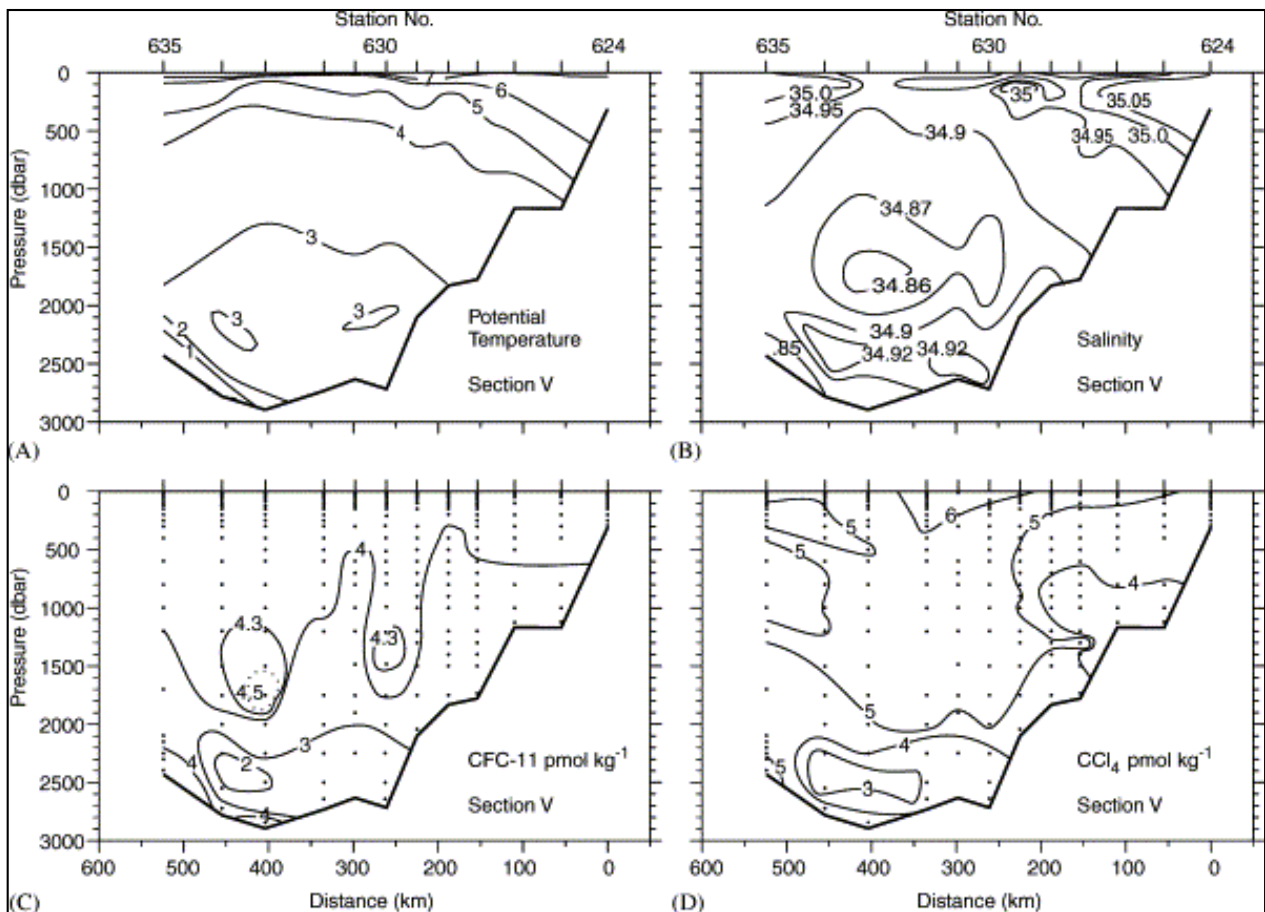


Fig. 7. Section V across the Irminger Basin from Reykjanes (Station 624) to the Greenland slope (Station 635). Distribution of (A) potential temperature, (B) salinity, (C) CFC-11, and (D) Ccl_4 .

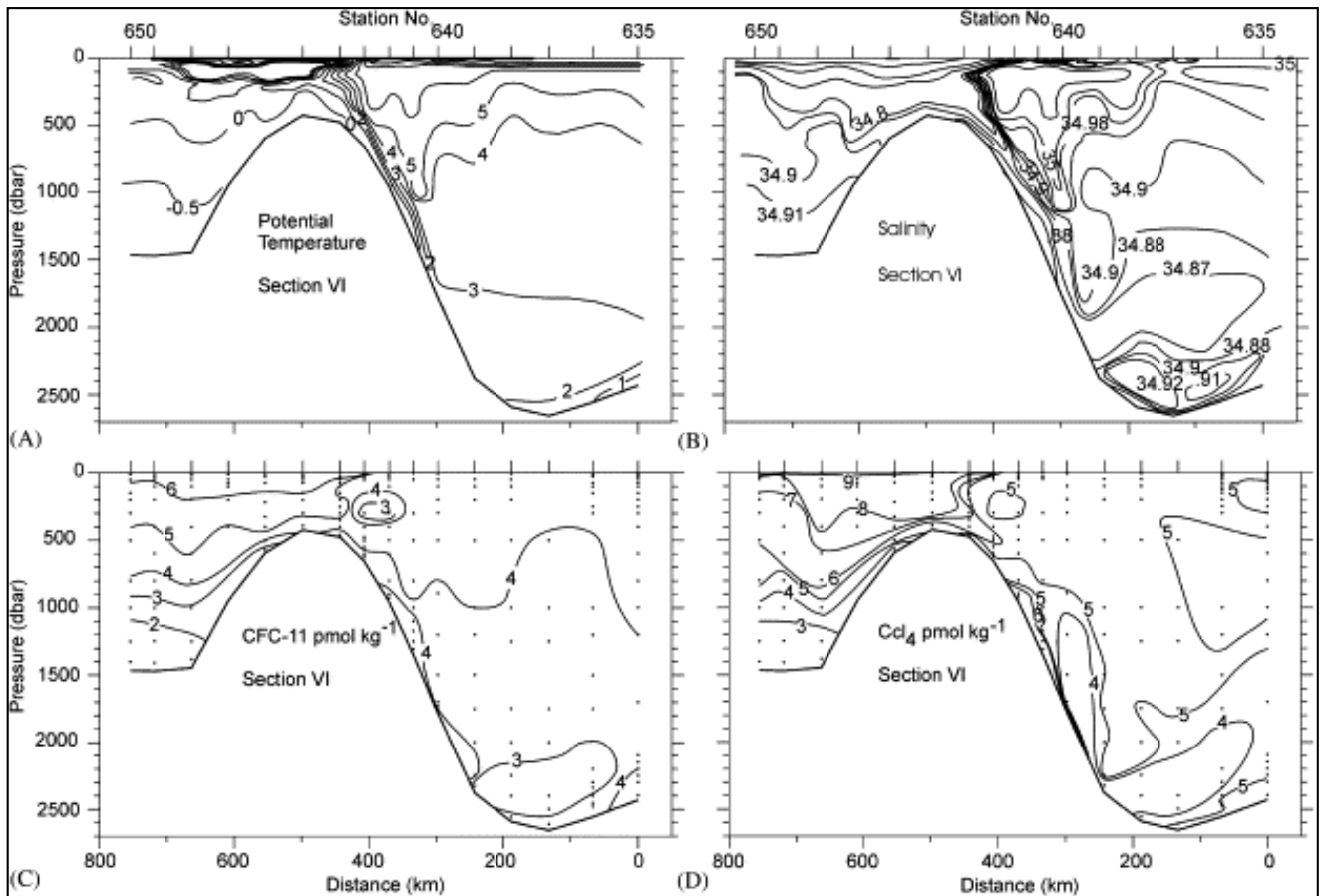


Fig. 8. Section VI through the Denmark Strait from the Irminger Basin (Station 635) to the Iceland Sea (Station 650). Distribution of (A) potential temperature, (B) salinity, (C) CFC-11, and (D) Ccl_4 .

The physical and chemical properties of the water masses that are compiled in [Table 1](#) are based mainly on the observations and data from the cruise in 1994 ([Fig. 1](#)). In a few cases supporting tracer data from other sources are used as indicated in the table. All the water masses in [Table 1](#) are defined in earlier literature as referred to below. As entered in [Table 1](#), the characteristics of LSW in the Iceland and Irminger Basins differ significantly, and they are therefore described separately as LSW_E and LSW_W , respectively.

3.1. The Nordic Seas

Both deep and intermediate water masses formed in the Nordic Seas contribute to the overflow across the Greenland–Scotland Ridge. The Return Atlantic Water (RAW) derives partly from the Atlantic layer in the Arctic Ocean and partly from the West Spitsbergen Current. In the Fram Strait this relatively warm and salty water of Atlantic origin is partly advected into the EGC and partly into the cyclonic circulation in the Greenland Sea. Some intermediate water from the Greenland Sea gyre also mixes into the EGC (see e.g. [Helland-Hansen and Nansen, 1909](#); [Bourke et al., 1988](#); [Mauritzen, 1996](#); [Rudels and Rudels](#)). Over the East Greenland slope it flows parallel with and intrudes under the Polar surface waters of the EGC. In the Iceland Sea the RAW is warmest and saltiest between 300 and 500 m depth. Much of it diverts into the East Icelandic Current, but most of the remaining portion, which continues through the Denmark Strait, seems to feed the Denmark Strait overflow.

Advection of RAW to the surface layers of the cyclonic circulation in the Greenland Sea has been particularly important in this area where the ultimate cooling in the process of Greenland Sea Deep Water (GSDW) formation may take place. If the salinity in the surface water is sufficiently high, from either advection or salt rejection caused by ice formation, the cooled water may become dense enough to create convection that reaches the bottom.

Very little bottom water has been formed in the Greenland Sea since the early 1970s ([Clarke et al., 1990](#); [Bönisch et al.,](#)

1997). Instead, winter convection has been limited to varying intermediate depths, and intermediate water masses have been formed ([Blindheim, 1999](#)). It seems clear that this is the main source of the intermediate water that during the 1980s and 1990s spread isopycnally above the older deep waters in the Nordic Seas ([Blindheim et al., 2000](#)). During the 1980s it was identified as a salinity minimum between the Atlantic water and the deep water over the entire Norwegian Sea and defined as Norwegian Sea Arctic Intermediate Water (NSAIW; [Blindheim, 1990](#); [Clarke et al., 1990](#); [Hopkins, 1991](#)). It was also observed in the Faroe–Shetland Channel ([Martin, 1993](#), [Turrell et al., 1999](#)). Under similar oceanographic and atmospheric conditions, it is likely that such intermediate water occurred in the Norwegian Sea earlier, but there have not been any observations to detect it.

NSAIW has been spreading isopycnally in a layer centred around $\sigma_{\theta}=28.0 \text{ kgm}^{-3}$ without significant changes in density, but as it has gradually mixed into the upper deep water the density interval widened during the 1990s. In the southern Norwegian Sea it appears as a salinity minimum, $S<34.9$, $-0.5^{\circ}\text{C}<\theta<+0.5^{\circ}\text{C}$, between about 400 and 700 m depth ([Fig. 4](#)). It contributes considerably to the overflow through the FBC.

Some intermediate water with similar properties is also formed in the Iceland Sea by winter cooling, although intermediate water formed in the Greenland Sea probably also advects into the Iceland Sea and mixes into this water mass. [Swift and Aagaard \(1981\)](#) classified this as upper Arctic Intermediate Water, but we prefer to call it Iceland Sea Arctic Intermediate Water (ISAIW). The East Icelandic Current carries much of this intermediate water into the southwestern Norwegian Sea, where it contributes to the NSAIW.

Another intermediate water mass, North Icelandic Winter Water, was described by [Stefansson \(1962\)](#). He found that it is formed in the North Icelandic coastal area during winter by mixing of Atlantic water deriving from the North Icelandic Irminger Current and Arctic waters from the Iceland Sea. He stated that it might be variable in composition. While this water is carried eastward along the Iceland–Faroe Front over the northern slope of the Iceland–Faroe Ridge, it mixes with slightly different water masses in the East Icelandic Current to form MEIW as described by [Read and Pollard \(1992](#); see also [Hansen and Østerhus, 2000](#)). In the present data set the MEIW, defined by temperatures of $1\text{--}3^{\circ}\text{C}$ and salinities in the range $34.70\text{--}34.90$, was observed over the northern slope of the Faroe–Iceland Ridge in Section II ([Fig. 4](#)), where it was identified at 300–400 m depth. This water mass probably contributes considerably to the overflow across the ridge between the Faroes and Iceland.

[Aagaard et al. \(1985\)](#) and [Swift and Koltermann \(1988\)](#) stated that the Norwegian Sea Deep Water (NSDW) is a mixture of about equal parts of GSDW and Eurasian Basin Deep Water (EBDW) from the Arctic Ocean. Deep waters in the Norwegian Sea of temperatures below -0.5°C are often characterised as NSDW, but the adiabatically isothermal NSDW at depths greater than ~ 2500 m had in 1994 a potential temperature of -1.03°C and a salinity of 34.91. NSDW has traditionally been considered to be the main source water mass for the overflow across the ridges between Iceland and Scotland (e.g. [Lee and Ellett, 1965](#)).

In a climatic context it is important to have knowledge of the age of the water masses forming deep waters in the North Atlantic, that is, the time since it was at the surface and equilibrated with the atmosphere. The relatively low age of the NSAIW is reflected in its high CFC-11 content, $3.5\text{--}4 \text{ pmolkg}^{-1}$, which on the assumption of 100% saturation in the surface layer of the formation area suggests an apparent age of 16–18 years. It is, however, known that the CFC levels in the surface layer of the central Greenland Sea during the convection period is only 65–80% of saturation ([Tanhua, 1997](#)). An age of 18 years is thus an upper limit, and the apparent age of the NSAIW is between 6 and 16 years when the under-saturation of the Greenland Sea is accounted for.

The apparent ages of the deep waters in the Nordic Seas have been estimated by several researchers. [Bullister and Weiss \(1983\)](#) measured CFC-11 and CFC-12 in the Norwegian Sea in 1982. Their estimate for the residence time of deep water in the Greenland Sea with respect to exchange with surface water was about 40 years. Similarly, they estimated the time scale for exchange between the deep Greenland Sea and the deep Norwegian Sea to be 20–30 years. During the following decade, several authors estimated renewal times of similar magnitude for the GSDW ([Smethie et al., 1986](#); [Heinze et al., 1990](#); [Bönisch and Schlosser, 1995](#)). [Rhein \(1991\)](#) estimated a turnover rate for NSDW with respect to GSDW and EBDW of 12–15 years. Using ^{14}C data [Gislefoss \(1994\)](#) estimated NSDW to be at least 130 years older than GSDW. The reason for the discrepancy between ^{14}C age estimate and those from CFC tracers is differences in the time scales that can be resolved by the two different approaches. [Bönisch and Schlosser \(1995\)](#) made a compilation of CFC-11 and CFC-12 measurements in the Norwegian Sea in 1982 and 1989. From the present CFC data, supported by additional data collected in 1994 and 1995

(Fogelqvist et al., unpublished data), one can notice a weak trend of increasing concentrations in the bottom water of the Norwegian Sea from 1982 to 1995. CFC-11 increased from 0.16 to 0.30 pmolkg⁻¹ and CFC-12 from 0.10 to 0.25 pmolkg⁻¹. The ratios CFC-11/CFC-12 are all in the range 1.4–1.6, pointing to a time for equilibration in 1962–1964.

Because of their almost identical properties, the deep waters in the Iceland and Norwegian Seas have traditionally been considered to be the same water mass. However, particularly in the western Iceland Sea, the deeper strata may be characterised by deep waters from the Arctic Ocean as far south as the Denmark Strait (Buch et al., 1996; Rudels et al., 1999c). Therefore, we will treat them as separate water masses because of the slightly higher CFC content and higher salinity in the Iceland Sea Deep Water (ISDW) than in the NSDW. Although the higher salinity in the ISDW derives from the Arctic Ocean, the higher CFC content is due to admixture of Arctic intermediate waters, mainly in the Greenland Sea (Rudels and Rudels). The higher CFC content also indicates a shorter flushing time of the Iceland Sea than of the Norwegian Sea. The bottom water in the Iceland Sea has CFC-11 and CFC-12 concentrations in the range of 1.1–1.2 and 0.51–0.52 pmolkg⁻¹, respectively, and a CFC-113 content below the limit of detection, which indicates an apparent age of the ISDW of more than 25 years (assuming 100% saturation). The water characteristics change gradually from the bottom towards the surface, and the properties of the water mass change from ISDW to those of more rapidly ventilated intermediate water and low salinity surface waters probably derived from the EGC (Fig. 8).

The central Iceland Sea has been mentioned as source area for DSOW because it is formation area of ISAIW. In several studies this type of intermediate water has been pointed out as the major source of the DSOW (Swift et al., 1980; Swift, 1984b; Livingston et al., 1985). More recent studies claim, however, that DSOW is formed by mixing within the EGC while being carried into the Denmark Strait. On the sill it forms a stratified plume, its deeper and denser portion being a mixture of RAW, including water from the Atlantic layer in the Arctic Ocean, and ISDW. The less dense part of the plume derives from the upper layers of the EGC, with Polar Intermediate Water as a main component (Strass et al., 1993; Rudels et al., 1999a).

From age determinations Smethie and Swift (1989) concluded that there had to be two types of DSOW, a low salinity type of an apparent age of 1.8 years or less, and a slightly higher salinity, more dense type, estimated at an age of 15–16 years. In spite of the confusion about source water masses, their age determinations may not be in conflict with the more recent results. They are also well in line with the ages determined here.

3.2. Faroe Bank Channel

In Section I (Fig. 3) across the FBC, the water close to the bottom had characteristics, $\theta = -0.51^\circ\text{C}$ and salinity 34.905, that, according to the definitions in Table 1, fall in the transition zone between NSAIW and NSDW. This gives ISOW near the bottom a potential density of $\sigma_\theta = 28.055 \text{ kgm}^{-3}$ ($\sigma_2 = 37.397 \text{ kgm}^{-3}$). It should, however, be noted that these characteristics represent the situation at the time when the section was occupied. Temperature data from Acoustic Doppler Current Profilers (ADCPs) deployed near the bottom in the channel over several years (Nordic WOCE Group, unpublished data), show considerable variations with time scales down to a few days, $t = -0.43 \pm 0.32^\circ\text{C}$. This indicates varying admixture of NSDW into the layer of NSAIW.

During the past two decades there must also have been slight changes on longer time scales in the properties of the NSDW in its source area, the Norwegian Basin. Because of increasing admixture of NSAIW mainly generated by year-to-year variations in the depth of winter convection in the Greenland Sea, the upper layers of the NSDW have gradually become slightly warmer and fresher. Such mixtures of NSDW and NSAIW flow into the deeper layers in the FBC. Similar characteristics are found in the southern part of the Norwegian Sea at depths between about 700 and 1000 m depth. According to the MVA, it is a mixture of about 50% NSDW and 50% NSAIW.

Historically, NSDW was considered to be the principal overflowing water mass (e.g. Lee and Ellett, 1965), and overflow water as observed in the FBC has been defined by the properties $\theta < 3^\circ\text{C}$, $S < 34.94$, but perhaps most generally in terms of density with $\sigma_\theta > 27.8 \text{ kgm}^{-3}$ (Hansen and Østerhus, 2000). The present data point to a layer of density $\sigma_\theta = 27.86\text{--}27.88$ ($\sigma_2 = 37.00\text{--}37.01$) as the border zone between the overflow water and the overlying basin waters. This density layer is associated with $\theta = 3^\circ\text{C}$ and $34.97 < S < 34.99$ along the whole pathway from the FBC to Section IV.

Based on CFC-11, CFC-12, tritium and ⁸⁵Kr measurements from 1981 and 1982, Smethie (1993) estimated the age of overflow water in the FBC to be 45 years. At that time, when the admixture of NSAIW into the upper layers of the NSDW was small, the densest overflow water would have had a considerably higher apparent age than the overflow in 1994.

Over the sill of the FBC (Fig. 3), it was possible to distinguish between some of the water masses flowing in from the Norwegian Sea. The water nearest the properties of NSDW was indicated by salinities above 34.9 in the bottom layer. Next above it was a layer of NSAIW, although with a contribution of MEIW. This was indicated by higher halocarbon concentrations, lower salinity and higher temperature. In the shallower layers of the overflow water, there was a sharp gradient in both temperature and salinity towards the overlying Atlantic Water, but mixing within the FBC as well as in the Faroe Shetland Channel (FSC) seems intense. Compared with the conditions farther east in the FSC, the NSAIW signal above the bottom layer in the FBC is considerably weakened, and the signature of MEIW is at least periodically wiped out by mixing with the Atlantic water above (Hansen and Østerhus, 2000). Because of this intense mixing, the features indicating different water masses as seen in Fig. 3, may be broken down in, or shortly downstream of, the channel. Within the FBC a main reason is the high speed of the plume. The current measurements show that annual means of the speed often exceed 1.1 ms^{-1} (Hansen and Østerhus, 2000). This creates intensive mixing in the boundary layers of the plume. At the interface between the overflow water and the overlying Atlantic Water, the shear is strong enough to result in instabilities and considerable mixing. Hence, Richardson numbers based on the mean annual current velocity profiles, and the typical density profile in the channel, are below 0.5 between 500 and 600 m depth and with a minimum of less than 0.25 around 550 m depth. Most likely, instabilities observed between 630 and 650 m depth in the CTD observations on Section I results, therefore, from velocity shears. Furthermore, as previously stated by Johnson and Sanford (1992), the high velocity creates a large bottom drag and a relatively thick bottom Ekman layer with high cross-stream current velocities. Preliminary analysis of the current meter data gives mean cross-stream velocities exceeding 0.3 ms^{-1} 40 m above the bottom. When the approximately 200 m high and 10 km wide plume of overflow water leaves the FBC, it will therefore quickly become wider, loose height and gain along-stream density gradients due to the high cross-stream velocities. This will contribute considerably to intensifying the mixing.

The description above shows that NSAIW is a principal water mass in the overflow through the FBC. A result of this is that the ISOW has become slightly warmer, slightly less saline and accordingly less dense since the early 1980s. This is, however, of little importance for the properties of the overflow water further downstream, which depend more on the greater fluctuations in the properties of the entrained waters than on small variations in the source waters flowing through the channel (Price and O'Neil Baringer, 1994). Based on the density reduction, there are estimates of a reduced flux through the FBC (Hansen et al., 2001). However, bearing in mind that little or no GSDW has been formed since the early 1970s (Schlosser et al., 1991; Bönnisch et al., 1997), this indicates that the thermohaline circulation across the Iceland–Scotland Ridge may be maintained, although somewhat reduced, also by intermediate waters as the overflowing water mass.

3.3. Iceland Basin

In the Iceland Basin the ISOW descends from a bottom depth of approximately 850 m in Section I to a depth of about 2300 m in Section IV. During this descent the ISOW mixes vigorously with the overlying water masses along its pathway. As indicated in Fig. 3, much of the overflow water has the characteristics of NSAIW or a mixture of NSAIW and NSDW with $\theta < 0.5^\circ\text{C}$, S near 34.90 and $\sigma_\theta > 28.0$. These characteristics change quickly when the overflow water has passed through the FBC. Although some overflow, mainly of MEIW, may have been added to the plume of overflow water after crossing the ridge west of the Faroes, the mixing with overlying Atlantic water is the dominating process. Hence, in Section II, which crosses the Faroe–Iceland Ridge only about 180 km west of Section I, its core properties have changed to $\theta = 2^\circ\text{C}$ and $S = 34.97$, and the potential density has decreased to about $\sigma_\theta = 27.95 \text{ kgm}^{-3}$. In Section II the overflow water is observed between about 900 and 1200 m depth, where it is distinguishable by low values in both temperature and salinity compared with the overlying Atlantic waters.

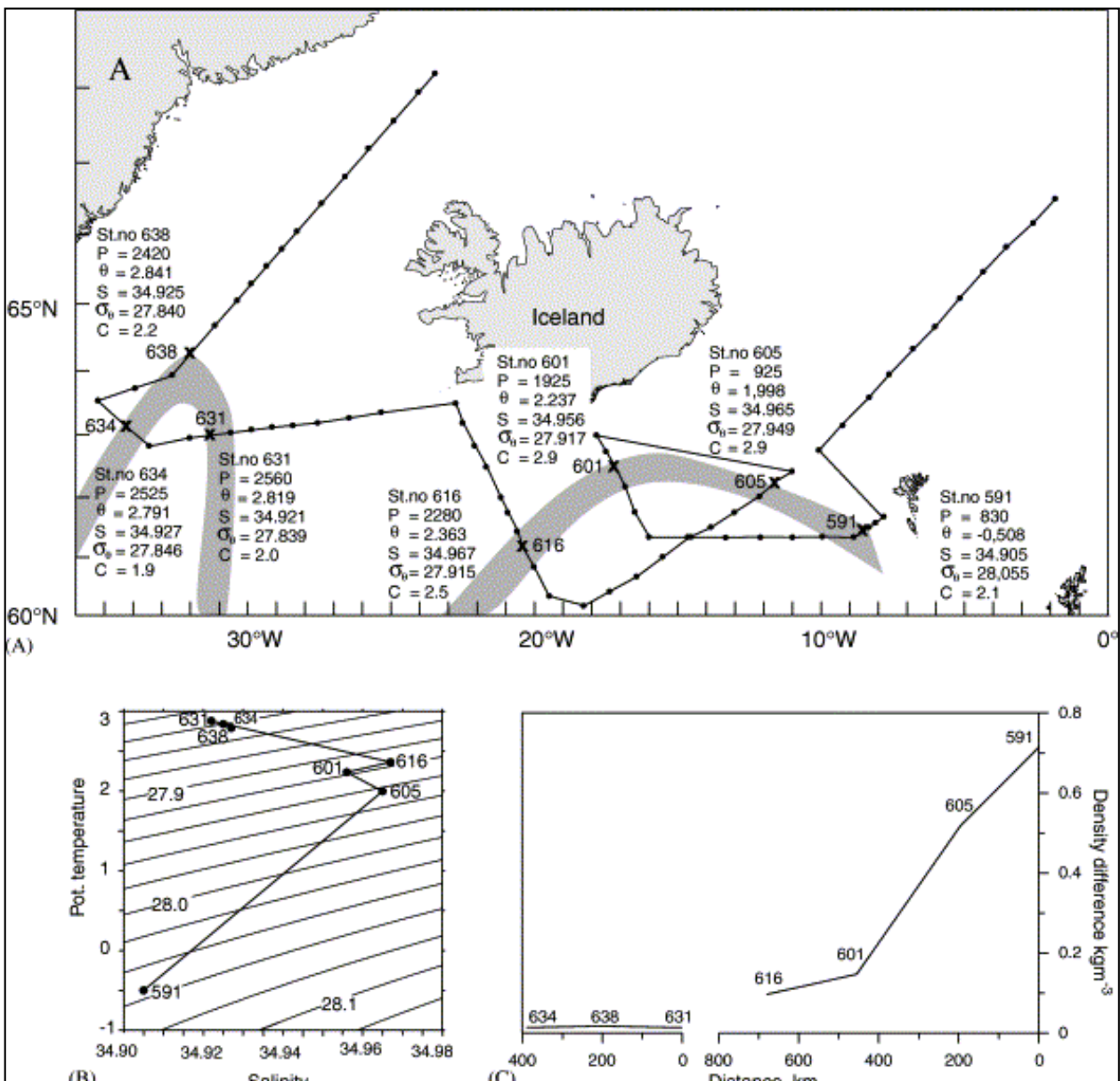
MVA of the overflow water in Section I (ISOW-II) indicates that it is a mixture of approximately 60% of the FBC bottom water (ISOW-I), 25% NEAW and 15% MEIW. Here the 60% ISOW-I may be split into 30% NSDW and 30% NSAIW, but it is not possible to determine the fractions of MEIW and NSAIW that have been flowing through the FBC or, alternatively, directly across the ridge west of the Faroes. It is, however, likely that some NSAIW and probably most of the MEIW took the western route over the ridge.

During the descent, three different water masses, NEAW, LSW_E and NEADW, mix with the ISOW to various degrees and in different depth layers. Resolution of the mixing between Sections I and IV by MVA was therefore not regarded reliable. However, a procedure in three steps between Sections I and IV gave more trustworthy results and also offered an indication of the development of the product of the mixing or entrainment along the main pathway of the overflow in the Iceland Basin. The results of the first step, between Sections I and II, have already been described above. In this first step the deeper portion of the overflow water in Section I was considered as one of the source water masses (ISOW-I) in the MVA, and the water in

the core of the overflow in Section II (ISOW-II) was considered as the product water. In the next step, ISOW-II was taken as one of the source water masses, and the core properties in Section III were considered to represent the product water mass. Accordingly, these properties in Section III defined one of the source water masses in the third step. The properties of ISOW-I, ISOW-II, ISOW-III and ISOW-IV that were applied in the multivariate analyses are entered in Table 4. These values represent properties observed at two–three stations in the overflow plume, below the bordering layer towards the overlying basin waters. As described above, this layer is characterised by densities between 27.86 and 27.88 kgm^{-3} , temperatures near 3°C, and salinities of 34.97–34.99. The values that are entered in Fig. 9 show the observations nearest to the bottom at one station in the centre of the plume and are in agreement with those in Table 4.

Table 4. Properties of waters in the overflow plume applied in the multivariate analysis of overflow waters in the sections in the Iceland Basin

	Units	ISOW-I	ISOW-II	ISOW-III	ISOW-IV
S		34.9	34.97	34.95–34.98	34.96–34.97
θ	°C	-0.51	1.95	2.3–2.7	2.4–2.7
O_2	$\mu\text{mol kg}^{-1}$	296.6	282–287	280–284	276–279
SiO_2	$\mu\text{mol kg}^{-1}$	9.9	8.7–9.7	9.3–10.0	10.5–11.5
NO_3	$\mu\text{mol kg}^{-1}$	15.2	13.7–14.2	14.7–15.0	14.7–15.0
PO_4	$\mu\text{mol kg}^{-1}$	1.07	1.02–1.07	1.08–1.10	1.09–1.12
CFC-11	pmol kg^{-1}	2.06	2.7–2.9	2.8–3.0	2.4–2.6
CFC-12	pmol kg^{-1}	0.93	1.20–1.25	1.2–1.4	1.0–1.2
CFC-113	pmol kg^{-1}	No data	0.15–0.17	0.2	0.15–0.18
CCl_4	pmol kg^{-1}	3.3	3.9	3.6–4.0	3.3–4.0



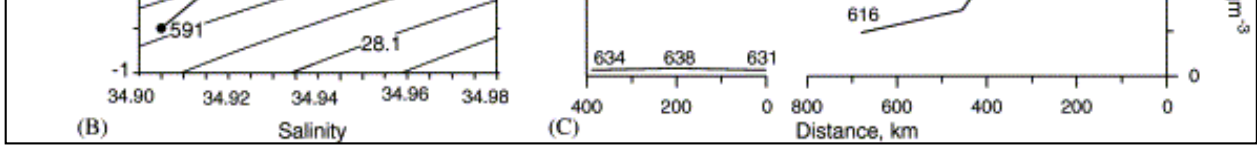


Fig. 9. (A) Some core properties (pressure, potential temperature, salinity, potential density, content of CFC-11 which is called C in the figure) in the plume of Iceland–Scotland Overflow Water (ISOW) at stations indicated by X and station number. (B) θ –S relationship of values entered in A. (C) Difference between in situ density associated with the values entered in A and in situ density at the same pressure at stations more centrally in the basins, away from the plume, average of Stations 597 and 609 in the Iceland Basin and Station 632 in the Irminger Basin.

Although the chemical components are not strictly conservative variables, they may still be applied in the MVA. At depths less than 2000 m, current velocities in the core of the overflow are measured at about 0.19 ms^{-1} , and they are approximately 0.1 ms^{-1} at greater depths further downstream (Saunders, 1996; Van Aken, 1995). For example between Sections II and III, which are spaced 300 km apart, propagation time would consequently vary between about 3 weeks and, very approximately, 4 months depending on speed and pathway length. The none-conservative character of the nutrients and the transient tracers seems, therefore, to be acceptable for the accuracy of the analysis. The CFC values applied in the MVA were all determined during the survey in 1994.

The evolution of the ISOW within the Iceland Basin is indicated in Fig. 9. Pressure, potential temperature, salinity, potential density and content of CFC-11 near the bottom at stations that hit the core of the ISOW in the various sections are entered in Fig. 9A, and the inset θ /S relationship in Fig. 9B shows the development of the ISOW in the θ /S space. Fig. 9C shows the development of the density difference between these core waters and the basin waters at the same pressure level as represented by the mean values based on Stations 597 and 609 (see Fig. 1). This yields an indication of the buoyancy forcing acting on the plume water of the various sections.

In Section III across the slope south of Iceland (Fig. 5), the main core of ISOW was observed around 17°W , where it was observed near the bottom at Station 601 (Fig. 9A). At this station it was identified at about 1900 m depth by its relatively low potential temperature, below 2.5°C . Although this is a low temperature in relation to the surroundings, it represents a rise of about 0.5°C from Section II while the salinity has decreased slightly to 34.96. The mixing and entrainment by the ambient water is therefore best reflected in the considerable temperature rise, while the moderate salinity change just shows that the salinity of the ISOW in these depth layers is not much different from the salinity of the ambient water. The small change in salinity is therefore not due to a low mixing rate, but rather it indicates admixture of Labrador Sea Water (LSW_E) during the descent from 1200 to 1900 m depth. This is also the result if the MVA is taken a step further along the pathway, with ISOW-II as a source water mass. The model stabilises best with only LSW_E as an additional source water, and the resulting product water in the core of the plume in Section III consists of about 80% ISOW-II and 20% LSW_E . This corresponds to 48% ISOW-I, 20% NEAW, 12% MEIW and 20% LSW_E .

Section IV (Fig. 6) south of Reykjanes cuts through the ISOW plume at about 20°W , where the main core is found around 2300 m depth. Compared with Section III, about 220 km to the northeast, there is a temperature rise of 0.1°C , and there is also a slight salinity increase, which reflects the increasing salinity in the NEADW underneath the LSW_E . MVA with the plume water in Section III as a source water (ISOW-III), together with LSW_E and NEADW, indicates that the core of the plume in Section IV is composed of 90% ISOW-III, 7% LSW_E and 3% NEADW, which is the same as 43% ISOW-I, 18% NEAW, 11% MEIW, 25% LSW_E and 3% NEADW.

This represents a considerably reduced mixing in relation to the two steps further upstream. Although the slope over which the plume descends is steeper than that between Sections I and II, the density difference between the plume water and the basin water, averaged between Sections III and IV, is reduced to 0.122 kgm^{-3} , or $\frac{1}{8}$ of the initial in the FBC. The buoyancy forcing is reduced accordingly, and, as seen in Fig. 9B, in contrast to the diapycnal mixing further upstream, it results in almost isopycnal mixing between Sections III and IV.

Multivariate analysis has its limitations, and the resulting fractional values should be considered with caution. In general, however, it may be concluded that it is a quantitative method that, in cases where different water masses have small differences in temperature and salinity, is more reliable than a plain T/S analysis. The results show that mixing was more vigorous between Sections I and II than between the other sections with the plume at greater depths. Hence, the amount of the original FBC bottom water per unit volume was reduced by 40% between Sections I and II, and the reduction from there to

Section IV was approximately a further 20%. The residual of 40% of original ISOW in the core of the plume on Section IV can hardly be interpreted as an approximate doubling of the volume of the plume, because there may also have been some "detrainment" of plume water out into the ambient water masses along the pathway. It is further worth noting that the fraction of NSDW in Section IV was of similar size as the fraction of NEAW, close to 20% each. In comparison to a potential density relative to 2000 dbar of $\sigma_2=37.397 \text{ kgm}^{-3}$ in the FBC, its value was $\sigma_2=37.093 \text{ kgm}^{-3}$ in the core of the ISOW plume in Section IV.

The fraction of original ISOW in the product water in Section IV is in good agreement with the results obtained by Harvey and Theodorou (1986), who, from a θ -S-O₂ analysis of historical data, estimated the fraction of original ISOW to be 40–45%. Also modelling results presented by Price and O'Neil Baringer (1994) are in support of these results. The results of the multivariate analyses, however, yield more details in the fractional composition of the plume water along the path of the overflow and also indicate where the most intensive entrainment occurs. The results show that the entrainment between Sections III and IV was small compared with the next step upstream, and particularly in comparison to the first step between Sections I and II.

In most cases the rate of mixing through entrainment is largest in areas with highest current speed. As stated, for example, by Price and O'Neil Baringer (1994), the speed of an overflow current is determined largely by the density difference between the overflow water and the overlying oceanic water, the bottom slope and the Coriolis parameter. In the present case, the Coriolis parameter may be considered as constant between Sections I and IV. The steepest topography occurs between Sections II and III, and although the density difference decreases considerably with increasing depth, its average value between these two sections is 0.33 kgm^{-3} . The forcing of the overflow current, the buoyancy acceleration, which is a product of the bottom slope and the density difference, therefore has its greatest magnitude between these two sections, more than thrice that between Sections I and II. The relatively high rate of mixing between Sections I and II can therefore not be due to the buoyancy acceleration. Neither does it seem likely that it depends on bottom roughness, since the structure of the bottom between Sections I and II is not known to be significantly different from the roughness between Sections II and III. Probably, the main reason is the high speed of the plume through the FBC that is described above. Mainly because of the high cross-stream velocities, the plume will collapse when it leaves the FBC. This will contribute considerably to intensifying the mixing, and it may further favour the diversion to the southwest of some overflow water just west of the FBC as indicated by Müller et al. (1979).

Although the density of the ISOW seems to have remained nearly constant during the past four decades, it seems clear that salinity and temperature have varied. In a section approximately along 60°N in 1955, Dietrich (1957) reported salinities of 35.00 in the ISOW. In 1960, Steele et al. (1962) observed salinities of up to 35.04 in a section southeast of Iceland at about the location of Section III. Since then the salinities in the core of the ISOW have gradually decreased, to 34.98 in 1981 (Swift, 1984a) and in 1991 (Bersch et al., 1999), and to 34.96 in 1994 as shown by the present data.

Although the observations referred to above cover somewhat various locations along the pathway of the ISOW, it is clear that salinities were higher around 1960 than during the later years. This is not surprising, since temperatures and salinities in both NEAW and LSW were higher at that time than during the later years (compare e.g. Section II with Steele et al., 1962). Bersch et al. (1999) showed that the water mass distribution in the northern North Atlantic varies with the atmospheric forcing. With the composition of the ISOW as indicated by the MVA in Section IV, a salinity change of 0.01 in the core of the ISOW would require a change of 0.06 in the NEAW, all other fractional properties kept constant. The observed variability in NEAW and LSW_E is therefore sufficient to result in the fluctuations that have occurred in the ISOW (Turrell et al., 1993; see also Dietrich, 1957).

The NEADW, characterised by high silicate and low oxygen contents as well as low tracer values (indicating an Antarctic influence), is most evident at the bottom of Station 613, with a silicate concentration of $17 \mu\text{molkg}^{-1}$, CFC-11 and CFC-12 concentrations of 1.7 and 0.8 pmolkg^{-1} , respectively, and oxygen concentrations less than $270 \mu\text{molkg}^{-1}$. The NEADW can be traced further to the northeast at Stations 612–609 and at Stations 597–598 along the eastern slope of the basin. The plume of NEADW can also be traced on the northwest slope of the Iceland Basin at Stations 599–600 and Stations 616–617. Here, the silicate values are lower and the halocarbons higher, suggesting entrainment during its cyclonal circulation around the Iceland Basin.

A distinctive core of LSW_E was recognised by its low salinity (~ 34.9) at depths of about 1400–1700 m in the central part of the basin. This was observed on Section II (Stations 609–613), Section III (Stations 597–600) and Section IV (Stations 613–

616). Wallace and Lazier (1988) report, from measurements made in 1986, that the LSW is significantly under-saturated (60% saturation) with respect to CFCs, but this is likely to be variable from 1 year to the next because of varying depths of the mixed layer, as demonstrated by Haine and Richards (1995), and the surface boundary conditions of the compounds (Jia, 1996). Doney and Bullister (1992) found the age of the LSW core in the Iceland Basin to be 10–11 years, based on the assumption of 60% saturation in the Labrador Sea during formation. From concentrations of CFCs, Min (1999) concluded that the spreading time for LSW to the Iceland Basin is 6–10 years. Our CFC values (2.2–2.4 pmolkg⁻¹ for CFC-11, 1.0 pmolkg⁻¹ for CFC-12 and 0.08 pmolkg⁻¹ for CFC-113) suggest, assuming 60% saturation as reported by Wallace and Lazier (1988), that this water was equilibrated at the surface in the late 1970s in the Labrador Sea. Also, the CFC-113/CFC-11 ratio, which is less sensitive to the degree of saturation, points to an age of 15–16 years, assuming equal saturation for the two tracers. Sy et al. (1997) observed CFC-11 concentrations in newly formed LSW in the Labrador Sea of 4.5 pmolkg⁻¹, which would indicate a saturation of about 77% that year. With 77% saturation applied to our data, the CFC-11 and -12 apparent ages would be about 3 years higher. Since the LSW core in the Iceland Basin is surrounded by water masses of slightly lower CFC values, any mixing with surrounding water masses would decrease the CFC content of the LSW core. Consequently, the estimate of 18–19 years is an upper limit for the transport time of LSW from the formation area to the central part of the Iceland Basin. The high CFC values (3.05 pmolkg⁻¹ for CFC-11 and 1.32 pmolkg⁻¹ for CFC-12) for recently formed LSW in 1986 reported by Wallace and Lazier (1988) have not yet reached the northern central part of the Iceland Basin, which would indicate a transport time of at least 8 years. Sy et al. (1997) report CFC-11 values of 2.8 pmolkg⁻¹ in the Iceland Basin during 1994 and argue that these CFC values indicate LSW vintages of 1986 or younger, after the onset of intense convection in the Labrador Basin. The position of that station is approximately 800 km southwest of where we found the core of LSW. For a mean speed of 1.5–2 cms⁻¹, as given by Sy et al. (1997), this corresponds to a transport time of about 1–1.5 years between the positions of the two observations. According to our data the onset of intense wintertime convection in the Labrador Sea in the late 1980s was thus not yet observed in the northern central part of the Iceland Basin in August 1994.

3.4. Irminger Basin

Three water masses dominate the deep water of the basin: ISOW, LSW_W and DSOW. The ISOW is found as a salinity maximum below the LSW_W while it flows above the colder and fresher DSOW in the western parts along the Greenland slope. Away from the sill, the densest water near the bottom has in the literature also been called Northwest Atlantic Bottom Water (e.g. Swift, 1984b). Sections V and VI are, however, so close to the Denmark Strait sill that we prefer to call it DSOW.

In Section V, approximately along 63°N across northern Irminger Basin (Fig. 7), the ISOW is observed between about 2200 and 2700 m depth, where it has spread in a layer with salinities above 34.9 across the basin. These are somewhat in contrast to the lower salinities of the LSW_W above and the DSOW below. The core of the flow is, however, clearly indicated by isolated cells with salinity above 34.92 both on the eastern side, at the foot of the Reykjanes slope, and on the western side, off the deeper Greenland slope. In Section VI, a similar core is observed off the deeper slope of the Greenland–Iceland Ridge. Assuming that the ISOW has crossed the mid-ocean ridge through the Charlie–Gibbs Fracture Zone, the length of its path from Section IV in the Iceland Basin is approximately 3000 km. Considering the vertical extent of the plume of ISOW in Section IV, it is possible that its shallower portions have passed through gaps further north on the Reykjanes Ridge. A crossing through the gap at about 55°N would shorten the path to approximately 2200 km. In any case, compared with the mixing during the descent further upstream, the rate of mixing is considerably reduced during the path around the Reykjanes Ridge, although the ISOW temperatures and salinities in Section V represent a freshening and warming compared with Section IV. Hence, the potential temperatures in the ISOW core off the Reykjanes slope in Section V, slightly above 3.0°C, are 0.5°C higher than the corresponding temperatures in Section IV. Similarly there is a salinity decrease of 0.04. This indicates that the LSW has been the dominant water mass in the mixing process around the Reykjanes Ridge, because the NEABW is mainly colder than the ISOW in Section V, and its salinity of 34.95–34.97 cannot cause the observed salinity reduction in the less saline ISOW.

Over the same distance the buoyant forcing of the ISOW is reduced from 0.1 kgm⁻³ in Section IV to 0.01 kgm⁻³ in the Irminger Basin, where Station 632 is applied as the "oceanic" reference. The density of the ISOW does not change much in the northern Irminger Basin, and the flow of the ISOW is, therefore, close to geostrophic and neutrally buoyant in this area. While it has been following the bottom along its entire path from the FBC, around the Reykjanes Ridge to Section VI, it is distinguishable as a salinity maximum above the DSOW in the western Irminger Basin. In support of this, the temperature and salinity of the ISOW in the southbound current on the western side of the Irminger Basin was nearly the same as on the eastern slope, indicating moderate mixing during its circulation around the northern Irminger Basin. Application of MVA on Stations 637 and 638 indicated that practically no DSOW mixed into the ISOW while it descended through the plume of

ISOW. Because of this, the ISOW also shows a reduced rate of change of density in this area. The slight increase is due mainly to a correspondingly small rise in salinity (Fig. 9A) that is not readily explainable by mixing since all surrounding basin waters are fresher. This is suggestive of temporal variability in the properties. Comparisons with previous studies show that such variations over longer time scales, similar to those in the Iceland Basin, are considerable also in the Irminger Basin. Hence, Dietrich (1957) reported on salinities in excess of 34.95 near the bottom along the western side of the Reykjanes Ridge in 1955. Further, Blindheim (1968) observed similar high salinities during the early 1960s. At Ocean Weather Station A (62°N, 33°W), where water samples were collected during five half-year periods from 1954 to 1963, inclusive, the salinities in the ISOW exceeded 34.97, while the overall average was 34.943. Hydrographic sections between OWS A and the Greenland coast in 1962–1964 all showed salinities above 34.95 in the ISOW, although its volume varied somewhat during this period. As in the Iceland Basin, these higher salinities in the ISOW must derive mainly from entrained NEAW, which in response to different atmospheric forcing was saltier in the late 1950s and the 1960s than in 1994. For the same reason, the volume of the Atlantic waters carried along the western side of the Reykjanes Ridge by the Irminger Current was also larger during the 1960s than in 1994 (Dietrich, 1957; Lee and Ellett, 1965; Blindheim, 1968; Kushnir, 1994; Belkin et al., 1998).

The transport time of ISOW between Station 601 in the Iceland Basin and Station 631 in the Irminger Basin is in the range 2–4 years, based on the absolute difference in the tracer concentrations (Fig. 9). This is a measure of the time of conveyance through the Charlie–Gibbs Fracture Zone. From the relation between ^3H and ^{85}Kr , Smethie and Swift (1989) estimated the propagation time of ISOW from the Iceland Basin through the Charlie–Gibbs Fracture Zone into the Irminger Basin to 1–11.5 years, with a best estimate of 7.5 years. Our data point is at the lower range of this estimate. Also, only small differences in CFC-11 and CCl_4 concentrations were noticed between the western and the eastern plume of ISOW within the Irminger Basin, indicating a circulation within the northern basin on a time scale of less than a year.

Also the LSW in the Irminger Basin was warmer, saltier and less prominent around 1960 than in 1994. During five half-year periods with observations at OWS A, the LSW was recognised by a minimum in salinity at about 1000 m depth. Its mean T/S core salinities were about 34.91 while the minimum salinity in the T/S core was the same in all periods, slightly above 34.88 with associated temperatures of 3.45–3.55°C (Blindheim, 1968). This is in contrast to the conditions experienced during 1994. Although Section V is further north than OWS A, it shows a fairly large core of LSW with salinities below 34.86. In spite of this salinity decrease, the density of the LSW has increased as a result of considerably lower temperatures. Consequently, the depth of the salinity minimum had also increased from about 1000 m around 1960 to about 1700 m in 1994. This cooling and freshening of the LSW is also reported in other studies based on different data (Brewer et al., 1983; Bersch et al., 1999; Mortensen and Valdimarsson, 1999).

From the tracer distribution and the CFC-113/CFC-11 ratio it can be deduced that the LSW_w at Stations 631–634 (Fig. 7) consists of two layers, a shallower layer at a depth of 1000–1500 m, which is older than the layer beneath at 1500–1800 m by about 4 years. The CFC-113 concentration in the upper layer is about 0.27 pmolkg^{-1} , whereas in the core of the lower layer the concentration is 0.35 pmolkg^{-1} . There is also a difference in the salinity and temperature between the two layers, the upper layer being warmer by about 0.2°C and its salinity lower by 0.01 units. Min (1999) used CFCs to determine transport of LSW in the North Atlantic, and he concluded that the shortest path from the source region to the central parts of the Irminger Basin is ~4 years. These findings are in contrast to the conclusions of Sy et al. (1997) who found transfer times from the Labrador Sea to the Irminger basin of 6 months. Our CFC-11 concentration in the deep core is close to 4.5 pmolkg^{-1} , which is the same value as Sy et al. (1997) found further south in the Irminger Basin and in the Labrador Sea later during the same year. Also the θ/S properties ($\theta=2.90^\circ\text{C}$, $S=34.86$) of the LSW core are close to and of the same density as their data from November 1994, although slightly warmer and saltier as may be expected since our Section V is about 300 km further north in the Irminger Basin. Sy et al. (1997) observed the LSW in November 1994, approximately 700 km from the central convection area; our observations are from early August 1994. If this LSW had been formed in March of the same year, it would require a spreading speed of at least 8 cms^{-1} to be advected the distance of approximately 1000 km to the northern Irminger Basin. This is almost twice the spreading speed of about 4.5 cms^{-1} that Sy et al. (1997) estimated for the LSW to reach the Irminger Sea some 6 months after its formation. Compared with other advective events, for example the Great Salinity Anomaly (Dickson et al., 1988), this is an extraordinarily high advection rate. It seems, therefore, questionable whether this LSW was formed in 1994. For 77% saturation of CFC-11 in the Labrador Sea, as reported by Sy et al. (1997), our CFC-11 values in the core of the LSW point to a vintage ranging from 1990 to 1994, the range of uncertainty being due to the nearly constant atmospheric CFC-11 concentration at that time. This range in time may allow spreading of LSW to the northern Irminger Basin by an even more moderate spreading speed than the 4.5 cms^{-1} that is reported on by Sy et al. (1997).

At the westernmost station of Section V, the temperature was below 0.5°C and the salinity below 34.85 near the bottom at

2430 m depth. By its potential temperature and salinity this is DSOW. Boluses of apparently pure overflow water more than 100 km downstream from the sill are a normal feature in the northern Irminger Sea that is mentioned in several publications. For example [Mann \(1969\)](#) and [Swift \(1984b\)](#) state that away from the sill the densest bottom water is always slightly less saline than the densest fraction of the DSOW at the sill although it replaces saltier waters during its descent. The reason for this seems to be the structure of the plume. Based on a larger data set from 1997, [Rudels and Rudels](#) conclude that the presence of a low salinity lid implies that entrainment of overlying basin waters is small and that the downstream evolution of the plume characteristics is due to mixing within the plume between the initial overflow waters.

The observation of similar conditions also in the single section across the ridge of the present data set ([Fig. 8](#)) suggests that this may be a frequently occurring overflow pattern. During much of the descent, particularly in the depth interval of the relatively salty waters of the Irminger Current, there is a buffering layer of fresher water above the denser fractions of DSOW. Although this water by itself is not dense enough to descend to the bottom, it mixes with the denser water below at the same time as it isolates the water next to the bottom from the saltier basin water above. This is demonstrated for example on Station 641 in Section VI. There the approximately 100 m thick, nearly homogeneous bottom layer ($\theta=0.3^{\circ}\text{C}$, $S=34.82\text{--}34.83$, bottom depth 1346 m) lies under an almost equally thick layer of considerably fresher water with a minimum salinity of 34.75, which is close in properties to Polar Intermediate Water (PIW). This water may be entrained into the bottom layer at the same time as it creates a considerable density shear towards the warmer and saltier water above.

Over the deeper slope where the buffering, fresher layer is absent, the properties of the surrounding waters, mainly LSW_w, are not much different from the properties of the plume water. Furthermore, the density difference between the plume water and the basin water at this depth is reduced to about half of the density difference at the sill level. Although the topography is steep also at this deeper part of the slope, the reduced buoyancy forcing will result in lower speed of the overflow current and reduced entrainment. The densest fraction of the overflow water therefore gets fresher by mixing with PIW immediately downstream of the sill. However, on its descent to greater depths of the basin, the DSOW increases in both salinity and temperature and gets lower in CFCs. MVA indicates that the plume of the DSOW at Station 635 has about 10% ISOW mixed into it. Here, it should be mentioned that a single along-stream section through the Denmark Strait might not capture the core of the overflow within the strait itself. We are, however, confident that the overflow plume was sampled on the slope south of the sill.

[Smethie and Swift \(1989\)](#) estimated the ages of DSOW in the Irminger Basin and identified two components of overflow water: a low salinity component with a maximum age of 1.8 years (upper Arctic Intermediate Water) and a high salinity component with a deeper source in the Iceland Sea (lower AIW; equivalent to RAW in our nomenclature, see [Table 1](#)) and with a tracer signal indicating an age of 15–16 years. [Livingston et al. \(1985\)](#) used the isotopes ^{137}Cs and ^{90}Sr together with ^3H for a study in the northern Irminger Basin. They concluded that the source of the low salinity component of the DSOW is upper AIW formed in the Iceland Sea, and that the transport over the sill takes about 2 years. As mentioned above, more recent studies argue that the source of DSOW is mainly the EGC ([Strass et al., 1993](#); [Rudels et al., 1999a](#)). The present data indicated that the DSOW, when entering the Irminger Basin, was composed of one-third of ISDW and about two-thirds less dense water, similar to ISAIW, but which well might have derived from the less dense part of the EGC. Multivariate analyses of the data from this area are, however, uncertain because of the many water masses involved, and one single section ([Fig. 8](#)) may also have sampled the area insufficiently. That might, furthermore, have been the reason why RAW was not observed in Section VI. Still, it seems that the present results support the findings presented by [Rudels et al. \(1999a\)](#).

The property of the ISOW that showed the greatest change along the path from the FBC to the East Greenland slope at 63°N , was its temperature. As illustrated in [Fig. 9](#), did the potential temperature increase by 3.3°C . Most of this change, 2.9°C , occurred in the Iceland Basin showing that most of the entrainment occurred there. The most intense mixing occurred between the FBC and Section II where admixture of NEAW raised the salinity in the ISOW plume to its maximum, 34.97. The major entraining component along the pathway was, however, LSW, which in Section IV was assessed to contribute 25% of the volume. Since we do not know the properties of waters overlying the plume further south around the Reykjanes Ridge sufficiently well, we have not applied MVA on the overflow plume at the western slope of the Reykjavik Ridge in Section V. Entrainment, probably of LSW, during this passage has, however, resulted in a temperature increase of almost 0.5°C . It seems, therefore, reasonable to conclude that the LSW percentage at Station 631 west of the Reykjanes Ridge was between 30% and 40%. Hence, the overflow water that passes across the Iceland–Scotland Ridge seems to intermix with about equal portions of overlying waters before it meets the DSOW in the northern Irminger Basin. In this mixture NSDW and NEAW contributed equally in 1994.

Acknowledgements

This work was partly financed through research contracts with the Nordic Council of Ministers and the Swedish Natural Science Research Council, which are gratefully acknowledged. Jane Strømstad provided oxygen and nutrient data, Britt-Marie Dahlberg analysed the salinity samples and Karen Gjertsen did most of the drawing. We owe them many thanks. We also would like to thank the captain and the crew of the R. V. "Johan Hjort" for their valuable work during the cruise.

References

Aagaard 1968. K. Aagaard , Temperature variations in the Greenland Sea deep-water. *Deep-Sea Research* **15** (1968), pp. 281–296.

Aagaard 1985. K. Aagaard, J.H. Swift and C.E. Carmack , Thermohaline circulation in the Arctic Mediterranean Seas. *Journal of Geophysical Research* **90** (1985), pp. 4833–4846.

Belkin 1998. I.R. Belkin, S. Levitus, J. Antonov and S.-A. Malmberg , "Great Salinity Anomalies" in the North Atlantic. *Progress in Oceanography* **41** (1998), pp. 1–68.

Bersch 1999. M. Bersch, J. Meincke and A. Sy , Interannual thermohaline changes in the northern North Atlantic 1991–1996. *Deep-Sea Research II* **46** (1999), pp. 55–75.

Blindheim 1968. J. Blindheim , Hydrographic investigations in the Irminger Sea in the years 1954–1964. *Fiskeridirektoratets skrifter, Serie Havundersøkelser* **14** (1968), pp. 72–97.

Blindheim 1990. J. Blindheim , Arctic intermediate water in the Norwegian Sea. *Deep-Sea Research* **37** (1990), pp. 1475–1489.

Blindheim 1999. Blindheim, J., 1999. Wind generated fluctuations in water mass structure in the Nordic Seas. ICES CM 1999/L:24, 11pp.

Blindheim 2000. J. Blindheim, V. Borovkov, B. Hansen, S.-Aa. Malmberg, W.R. Turrell and S. Østerhus , Upper layer cooling and freshening in the Norwegian Sea in relation to atmospheric forcing. *Deep-Sea Research I* **47** (2000), pp. 655–680.

Bönisch and Schlosser 1995. G. Bönisch and P. Schlosser , Deep water formation and exchange rates in the Greenland/Norwegian Seas and the Eurasian Basin of the Arctic Ocean derived from tracer balances. *Progress in Oceanography* **35** (1995), pp. 29–52.

Bönisch 1997. G. Bönisch, J. Blindheim, J.L. Bullister, P. Schlosser and D.W.R. Wallace , Long-term trends of temperature, salinity, density and transient tracers in the central Greenland Sea. *Journal of Geophysical Research* **102** C8 (1997), pp. 18553–18571.

Borenäs and Lundberg 1988. K.M. Borenäs and P. Lundberg , On the deep-water flow through the Faroe Bank Channel. *Journal of Geophysical Research* **93** (1988), pp. 1281–1292.

Bourke 1988. R.H. Bourke, A.M. Weigel and R.G. Paquette , The westward turning branch of the West Spitsbergen Current. *Journal of Geophysical Research* **93** (1988), pp. 14065–14077.

Brewer 1983. P.G. Brewer, W.S. Broecker, W.J. Jenkins, P.B. Rhines, C.G. Rooth, J.H. Swift, T. Takahashi and R.T. Williams , A climatic freshening of the Deep Atlantic North of 50°N over the past 20 years. *Science* **22** (1983), pp. 1237–1239.

Bu and Warner 1995. X. Bu and M.J. Warner , Solubility of Chlorofluorocarbon 113 in water and seawater. *Deep-Sea Research I* **42** (1995), pp. 1151–1161.

Buch 1996. E. Buch, S.-Aa. Malmberg and S.S. Kristmannsson , Arctic Ocean deep water masses in the western Iceland Sea. *Journal of Geophysical Research* **101** (1996), pp. 11965–11973.

Bullister and Weiss 1983. J.L. Bullister and R.F. Weiss , Anthropogenic Chlorofluoromethanes in the Greenland and Norwegian Seas. *Science* **221** (1983), pp. 265–267.

Clarke 1990. R.A. Clarke, J.H. Swift, J.L. Reid and K.P. Koltermann , The formation of Greenland Sea Deep Water: double diffusion or deep convection?. *Deep-Sea Research* **37** (1990), pp. 1385–1424.

Dickson 1988. R.R. Dickson, J. Meincke, S.-A. Malmberg and A.J. Lee , The Great Salinity Anomaly in the northern North Atlantic 1968–1982. *Progress in Oceanography* **20** (1988), pp. 103–151.

Dickson 1990. R.R. Dickson, E.M. Gimtrowicz and A.J. Watson , Deep-water renewal in the northern North Atlantic. *Nature* **344** (1990), pp. 848–850.

Dietrich 1957. G. Dietrich , Schichtung und zirkulation der Irminger—see im June 1955. *Berichte der Deutschen Wissenschaftlichen Kommission für Meeresforschung* **14** 4 (1957), pp. 255–312.

Doney and Bullister 1992. S.C. Doney and J.L. Bullister , A chlorofluorocarbon section in the eastern North Atlantic. *Deep-Sea Research* **39** (1992), pp. 1857–1883.

Dooley and Meincke 1981. H. Dooley and J. Meincke , Circulation and water masses in the Faroese Channels during Overflow '73. *Deutsche Hydrographische Zeitschrift* **34** (1981), pp. 41–54.

Ellett and Martin 1973. D.J. Ellett and J.H.A. Martin , The physical and chemical oceanography of the Rockall Channel. *Deep-Sea Research* **20** (1973), pp. 585–625.

Esbensen 1994. Esbensen, K., Schönkopf, S., Midtgaard, T., 1994. *Multivariate Analysis in Practice. Computer-Aided Modelling A/S*, Trondheim, Norway.

Fogelqvist 1999. E. Fogelqvist , Determination of volatile halocarbons in seawater. In: K. Grasshoff, K. Kremling and M. Ehrhardt, Editors, *Methods of Seawater Analysis* (3rd Edition ed.), Wiley-VCH, Weinheim, Germany (1999), pp. 501–519.

Gislefoss 1994. Gislefoss, J.S., 1994. Carbon profiles in the Nordic Seas. Ph.D. Thesis, Radiological dating Laboratory, Faculty of Physics and Mathematics, Norwegian Institute of Technology, Trondheim, Norway.

Haine and Richards 1995. T.W.N. Haine and K.J. Richards , The influence of the seasonal mixed layer on oceanic uptake of CFCs. *Journal of Geophysical Research* **100** (1995), pp. 10727–10744.

Hansen and Østerhus 2000. B. Hansen and S. Østerhus , North Atlantic–Nordic Seas exchanges. *Progress in Oceanography* **45** (2000), pp. 109–208.

Hansen 2001. B. Hansen, W.R. Turrell and S. Østerhus , Decreasing overflow from the Nordic Seas into the Atlantic Ocean through the Faroe Bank Channel since 1950. *Nature* **411** (2001), pp. 927–929.

Harvey and Theodorou 1986. J.G. Harvey and A. Theodorou , The circulation of Norwegian Sea overflow water in the eastern North Atlantic. *Oceanologica Acta* **9** (1986), pp. 393–402.

Heinze 1990. C. Heinze, P. Schlosser, K.P. Koltermann and J. Meincke , A tracer study of the deep water renewal in the European polar seas. *Deep-Sea Research* **37** (1990), pp. 1425–1453.

Helland-Hansen and Nansen 1909. Helland-Hansen, B., Nansen, F., 1909. The Norwegian Sea. Its physical oceanography based upon the Norwegian researches 1900–1904. Report on Norwegian Fishery

and Marine Investigations 2, Part 1, No. 2, 390pp.

Hinrichsen and Tomczak 1993. H.-H. Hinrichsen and M. Tomczak , Optimum multiparameter analysis of the water mass structure in the Western North Atlantic Ocean. *Journal of Geophysical Research* **98** C6 (1993), pp. 10155–10169.

Hopkins 1991. T.S. Hopkins , The GIN Sea—a synthesis of its physical oceanography and literature review 1972–1985. *Earth-Science Reviews* **30** (1991), p. 318.

Jia 1996. Y. Jia , On tracer-derived ages in the Atlantic Isopycnic model. *International WOCE Newsletter* **23** (1996), pp. 14–17.

Johnson and Sanford 1992. G.C. Johnson and T.B. Sanford , Secondary circulation in the Faroe Bank Channel outflow. *Journal of Physical Oceanography* **22** (1992), pp. 927–933.

Karstensen and Tomczak 1998. J. Karstensen and M. Tomczak , Age determination of mixed water masses using CFC and oxygen data. *Journal of Geophysical Research* **103** C9 (1998), pp. 18599–18609.

Knudsen 1898. Knudsen, M., 1898. Den Danske Ingolf-Expedition, Copenhagen. Første Bind, 2, Hydrografi, pp. 21–154 with 35 plates (in Danish).

Kushnir 1994. Y. Kushnir , Interdecadal variations in North Atlantic sea surface temperature and associated atmospheric conditions. *Journal of Climate* **7** (1994), pp. 141–157.

Lee and Ellett 1965. A. Lee and D. Ellett , On the contribution of overflow water from the Norwegian Sea to the hydrographic structure of the North Atlantic Ocean. *Deep-Sea Research* **12** (1965), pp. 129–142.

Lee and Ellett 1967. A.J. Lee and D. Ellett , On the water masses of the Northwest Atlantic Ocean. *Deep-Sea Research* **14** (1967), pp. 183–190.

Livingston 1985. H.D. Livingston, J.H. Swift and H.G. "Ostlund , Artificial radionuclide tracer supply to Denmark Strait overflow between 1972 and 1981. *Journal of Geophysical Research* **90** (1985), pp. 6971–6982.

Mackas 1987. D.L. Mackas, K.L. Denman and A.F. Bennet , Least squares multiple tracer analysis of water mass composition. *Journal of Geophysical Research* **92** (1987), pp. 2907–2918.

Malmberg 1972. Malmberg, S.-Aa., 1972. Intermediate polar water in the Denmark Strait—"Overflow" August 1971. ICES C.M. 1972/C:6, 6pp, with 11 figures.

Mann 1969. C.R. Mann , Temperature and salinity characteristics of the Denmark Strait overflow. *Deep-Sea Research* **16** Suppl. (1969), pp. 125–137.

Martens and Naes 1989. H. Martens and T. Naes *Multivariate Calibration*, Wiley, New York (1989).

Martin 1993. J.H.A. Martin , Norwegian Sea intermediate water in the Faroe–Shetland Channel. *ICES Journal of Marine Science* **50** (1993), pp. 195–201.

Mauritzen 1996. C. Mauritzen , Production of dense overflow waters feeding the North Atlantic across the Greenland–Scotland Ridge, Part 1: evidence of a revised circulation scheme. *Deep-Sea Research I* **43** (1996), pp. 769–806.

McCartney 1992. M.S. McCartney , Recirculating components of the deep boundary current of the northern North Atlantic. *Progress in Oceanography* **29** (1992), pp. 283–383.

- Min 1999. Min, D.-H., 1999. Studies of large-scale intermediate and deep water circulation and ventilation in the North Atlantic, South Indian and Northeast Pacific oceans, and in the East Sea, Sea of Japan. Using Chlorofluorocarbons as Tracers. University of California, San Diego, La Jolla.
- Mortensen and Valdimarsson 1999. Mortensen, J., Valdimarsson, H., 1999. Thermohaline changes in the Irminger Sea. ICES CM 1999/L:16, 11pp.
- Müller 1979. Müller, T.J., Meincke, J., Becker, G.A., 1979. Overflow '73: the distribution of water masses on the Greenland–Scotland Ridge in August/September 1973—a data report. Berichte aus dem Institut für Meereskunde an der Christian-Albrechts-Universität, Kiel, 172pp.
- Otto and van Aken 1996. L. Otto and H.M. van Aken , Surface circulation in the North-east Atlantic as observed with drifters. *Deep-Sea Research I* **43** (1996), pp. 467–500.
- Preisendorfer 1988. Preisendorfer, R.W., 1988. Principal component analysis in meteorology and oceanography. In: Mobley C.D. (Ed.), Developments in Atmospheric Sciences, Vol. 17. Elsevier, Amsterdam, The Netherlands.
- Price and O'Neil Baringer 1994. J.F. Price and M. O'Neil Baringer , Outflows and deep water production by marginal seas. *Progress in Oceanography* **33** (1994), pp. 161–200.
- Read and Pollard 1992. J.F. Read and R.T. Pollard , Water masses in the region of the Iceland–Faeroes Front. *Journal of Physical Oceanography* **22** (1992), pp. 1365–1378.
- Rhein 1991. M. Rhein , Ventilation rates of the Greenland and Norwegian Seas derived from distributions of the chlorofluoromethanes F11 and F12. *Deep-Sea Research* **38** (1991), pp. 485–503.
- Ross 1984. Ross, C.K., 1984. Temperature-salinity characteristics of the "overflow" water in Denmark Strait during "OVERFLOW" 73. ICES, Report 185, pp. 111–119.
- Rudels 1999a. Rudels, B., Fahrbach, E., Meincke, J., 1999a. The East Greenland Current from Fram Strait to Beyond Denmark Strait in 1998: observations from RV Polarstern and RV Valdivia. ICES, C.M. L:23.
- Rudels 1999b. B. Rudels, P. Eriksson, H. Grönvall, R. Hietala and Launiainen , Hydrographic observations in Denmark Strait in Fall 1997, and their implications for the entrainment into the overflow plume. *Geophysical Research Letters* **26** 9 (1999), pp. 1325–1328.
- Rudels 1999c. B. Rudels, H.J. Friedrich and D. Quadfasel , The Arctic circumpolar boundary current. *Deep-Sea Research II* **46** (1999), pp. 1023–1062.
- Saunders 1990. P.M. Saunders , Cold outflow from the Faroe Bank Channel. *Journal of Physical Oceanography* **20** (1990), pp. 29–43.
- Saunders 1996. P.M. Saunders , The flux of dense cold overflow water southeast of Iceland. *Journal of Physical Oceanography* **26** (1996), pp. 85–95.
- Schlosser 1991. P. Schlosser, G. Bönisch, M. Rhein and R. Bayer , Reduction of deep water formation in the Greenland Sea during the 1980s: evidence from tracer data. *Science* **251** (1991), pp. 1054–1056.
- Schmitz and McCartney 1993. W.J. Schmitz and M.S. McCartney , On the North Atlantic Circulation. *Review of Geophysics* **31** (1993), pp. 29–49.
- Smethie 1993. M.W. Smethie , Tracing the thermohaline circulation in the western North Atlantic using chlorofluorocarbons. *Progress in Oceanography* **31** (1993), pp. 51–99.

Smethie and Swift 1989. M.W. Smethie and J.H. Swift , The Tritium Krypton-85 age of Denmark Strait Overflow Water and Gibbs Fracture Zone Water just south of Denmark Strait. *Journal of Geophysical Research* **94** (1989), pp. 8265–8275.

Smethie 1986. M.W. Smethie, H.G. Ostlund and H.H. Loosli , Ventilation of deep Greenland and Norwegian seas: evidence from krypton-85, tritium, carbon-14 and argon-39. *Deep-Sea Research* **33** (1986), pp. 675–703.

Steele 1962. J.H. Steele, J.R. Barrett and L.V. Worthington , Deep currents south of Iceland. *Deep-Sea Research* **9** (1962), pp. 465–474.

Stefansson 1962. U. Stefansson , North Icelandic waters. *Rit Fiskideildar* **3** (1962), p. 269.

Strass 1993. V.H. Strass, E. Fahrbach, U. Schauer and L. Sellmann , Formation of Denmark Strait overflow water by mixing in the east Greenland current. *Journal of Geophysical Research* **98** (1993), pp. 6907–6919.

Swift 1984a. Swift, J.H., 1984a. A recent θ - S shift in the deep water of the northern North Atlantic. In: Hansen, J.E., Takahashi, T. (Eds.), *Climate Processes and Climate Sensitivity*. Geophysical Monograph 29, Maurice Ewing Volume, 5, 39–47.

Swift 1984b. J.H. Swift , The circulation of the Denmark Strait and Iceland–Scotland overflow waters in the North Atlantic. *Deep-Sea Research* **31** (1984), pp. 1339–1355.

Swift and Aagaard 1981. J.H. Swift and K. Aagaard , Seasonal transitions and water mass formation in the Iceland and Greenland Seas. *Deep-Sea Research* **28** (1981), pp. 1107–1129.

Swift and Koltermann 1988. J.H. Swift and K.P. Koltermann , The origin of Norwegian Sea deep water. *Journal of Geophysical Research* **93** (1988), pp. 3563–3569.

Swift 1980. J.H. Swift, K. Aagaard and S.-Aa. Malmberg , The contribution of the Denmark Strait Overflow to the deep North Atlantic. *Deep-Sea Research* **27** (1980), pp. 29–42.

Sy 1997. A. Sy, M. Rhein, J.R.N. Lazier, K.P. Koltermann, J. Meincke, A. Putka and M. Bersch , Surprisingly rapid spreading of newly formed intermediate waters across the North Atlantic Ocean. *Nature* **386** (1997), pp. 675–679.

Tanhua 1997. Tanhua, T., 1997. Halogenated substances as marine tracers. Ph.D. Thesis, Department of Chemistry, Göteborg University, Göteborg, Sweden.

Tomczak 1981a. M.A. Tomczak , A multiparameter extension of temperature/salinity diagram techniques for the analysis of non-isopycnal mixing. *Progress in Oceanography* **10** (1981), pp. 147–171.

Tomczak 1981b. M.A. Tomczak , An analysis of mixing in the frontal zone of south and north Atlantic central water of North-West Africa. *Progress in Oceanography* **10** (1981), pp. 173–191.

Tomczak and Large 1989. M. Tomczak and D.B. Large , Optimum multiparameter analysis of mixing in the thermocline of the Eastern Indian Ocean. *Journal of Geophysical Research* **94** C11 (1989), pp. 16141–16149.

Turrell 1993. Turrell, W.R., Devonshire, E., Payne, R., Slessor, G., 1993. Analysis of the historic time-series obtained in the Faroe–Shetland Channel. ICES CM 1993/C:29, 22pp.

Turrell 1999. W.R. Turrell, G. Slessor, R.D. Adams, R. Payne and P.A. Gillibrand , Decadal variability in the composition of Faroe Shetland Channel bottom water. *Deep-Sea Research I* **46** (1999), pp. 1–25.

Van Aken 1995. H.M. Van Aken , Mean currents and current variability in the Iceland Basin. *Netherlands Journal of Sea Research* **33** 2 (1995), pp. 135–145.

Van Aken and Eisma 1987. H. Van Aken and D. Eisma , The circulation between Iceland and Scotland derived from water mass analysis. *Netherlands Journal of Sea Research* **21** (1987), pp. 1–15.

Walker 2000. S.J. Walker, R.F. Weiss and P.K. Salameh , Reconstructed histories of the annual mean atmospheric mole fractions for the halocarbons CFC-11, CFC-12, CFC-113 and carbon tetrachloride. *Journal of Geophysical Research* **105** C6 (2000), pp. 14285–14296.

Wallace and Lazier 1988. D.W.R. Wallace and J.R.N. Lazier , Anthropogenic chlorofluoromethanes in newly formed Labrador Sea Water. *Nature* **332** (1988), pp. 61–63.

Warner and Weiss 1985. M.J. Warner and R.F. Weiss , Solubilities of chlorofluorocarbons 11 and 12 in water and seawater. *Deep-Sea Research* **32** 12 (1985), pp. 1485–1497.